Techniques for improving 3D resolution in microscopy

Zvi Kam

Weizmann Institute of Science, Rehovot, Israel

ANR Diamond workshop, Mulhouse Dec 2011

TELESCOPES

Magnification effect of concave gold-plated mirrors used by **Egyptian queens**
Phoenicians condensing sun-light with water-filled spherical glass bottles and crystals (Pliny).
Geometrical optics books were written by **Euclid, Hero and Ptolemy** - Alexandria school.
Studies of the physical nature of light by **Ibn al-Haytham**, the medieval Arab scholar.
Optics emerged into the **renaissance** with the development of telescopes and microscopes.
Since – larger and better mirrors – yet limit is not the optics…

Greeks named Mercury as the "Twinkling Star" attributed to godly action.
Aristillus, Timocharis, Hipparchus and Ptolmy : (3-2nd century BC)
catalogues of 1020 stars with brightness levels of 1-5

Tyson: First adaptive optical reflector by **Archimedes**…
gap til our times

Johannes Kepler, Tycho Brahe, Galileo Galilei, William Herschel and his sister Caroline etc:
better and larger telescopes used at "calm" nights.

MICROSCOPES

Magnifying effect of morning dew droplets bringing **Greeks** to describe cells in leaves
1655, **Hook** built his compound microscope leading immediately to the description of cells
1674, **Leeuwenhoek's** simple microscopes from glass beads, described protozoa and bacteria
1833, **Brown** describe the nucleus in orchids
1838, **Schleiden & Schwann** state the cell theory
1876, **Abbe** define and achieve the 2D diffraction limit in resolution of light microscopes
1876, **Flemming** described mitosis
1881, **Cajal** used stains to see tissue anatomy
1882, **Koch** launched microbiology
1898, **Golgi** describes the Golgi apparatus using Zeiss and Abbe's diffraction-limited microscope
1924, **Lacassagne** developed Autoradiograpy following Curie's discovery of Radioactivity
Live cells seen using **Lebedeff's** interference microscope, and **Zernike's** phase contrast
1941, **Coone's** fluorescent microscope
1975, **Ploem's** epifluorescent microscope
1990, Green Fluorescent Proteins and variants

Minsky, Boyde Brakenhoff scanning confocal
1988, **Agard & Sedat** 3D deconvolution microscopy

Methods to fight 3D imaging aberrations

"Classical" correction of spherical aberration
- Change of tube length
- Slide thickness
- Immersion medium refractive index tuning
- Refractive index matching (e.g. Glycerol)
- Correction collars

Depth aberration
- Depth-dependent deconvolution
- AO correction with apriory knowledge of the wavefront shift

Sample-induced aberration
- Prediction of PSF from refractive index map (DIC) – Ray tracing in n(xyz)
- Methods of AO control - Peter
- Inverse Sample
- Deconvolution after AO correction -> space invariant PSF

Methods of modeling the microscope PSF

A. HUYGENS- FRESNEL PRINCIPLE (wavelets)

$$E(\mathbf{p_0}) = -i/2\lambda \int_A E(A) \exp[i\mathbf{k}.\mathbf{r_0}]/r_0 \; K(\chi)\, dA \qquad K(\chi) \sim 1+\cos\chi$$

where the integration is over the area A, $k=2\pi/\lambda$ is the wave vector, E(A) is the amplitude, $\mathbf{r_0}$ (magnitudes r_0) is the vectors from dA to the point $\mathbf{p_0}$

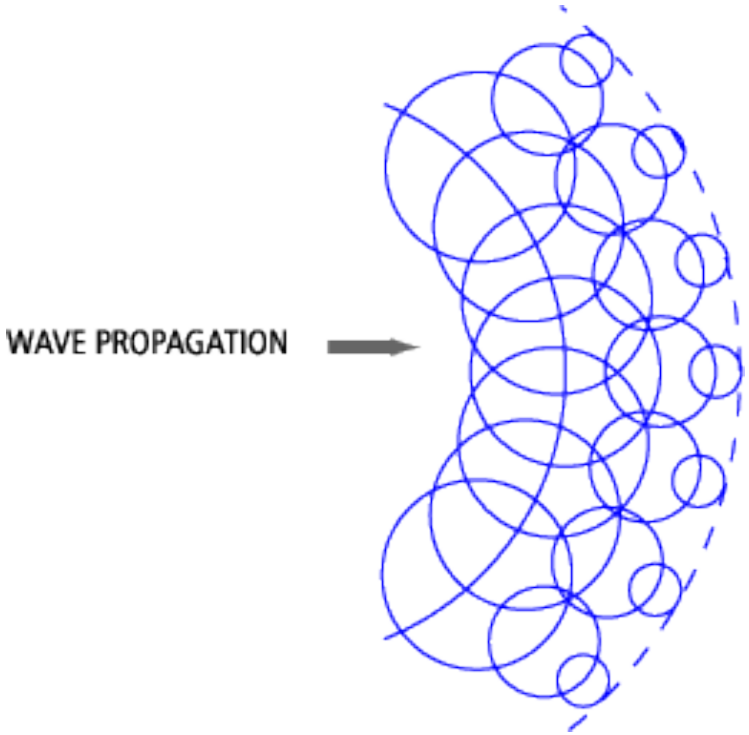

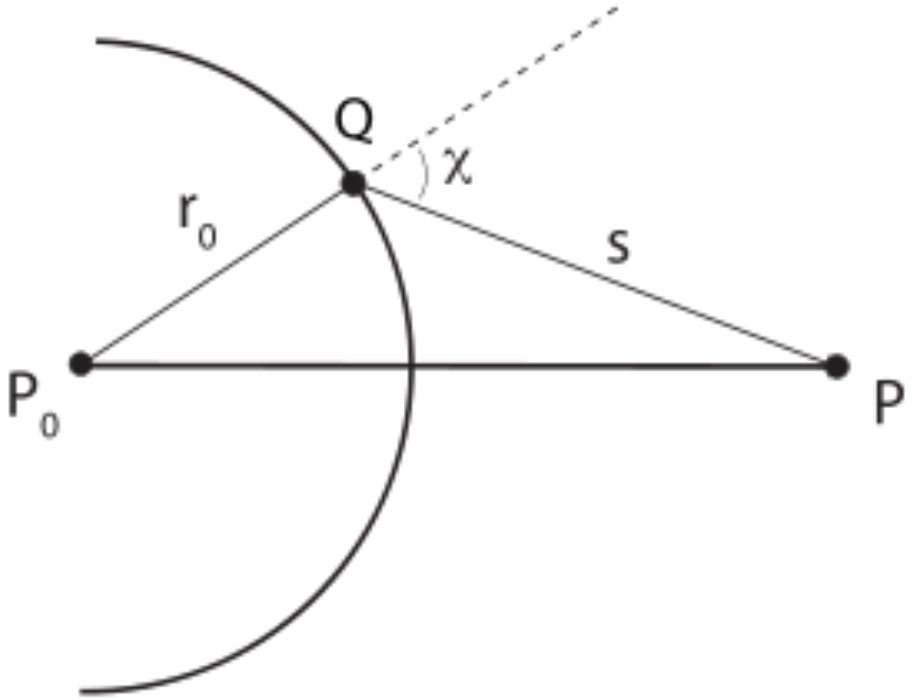

Methods of modeling the microscope PSF

B. FRESNEL-KIRCHHOFF-FRAUNHOFER DIFFRACTION INTEGRAL

$$E(\underline{\mathbf{p}}) = -i/2\lambda \int_A E(A) \exp[i\, \underline{\mathbf{k}}.\, (\underline{\mathbf{r}}+\underline{\mathbf{s}})+\varphi(A)]/rs \,*[\cos(\underline{\mathbf{n}}\hat{}\underline{\mathbf{r}})-\cos(\underline{\mathbf{n}}\hat{}\underline{\mathbf{s}})]\, dA$$

where the integration is over the exit pupil aperture A, $k=2\pi/\lambda$ is the wave vector, φ is the wavefront phase, E(A) is the energy and $\underline{\mathbf{n}} = \underline{\mathbf{n}}(A)$ is the unit vector normal to the wavefront at the intergation area element, dA, $\underline{\mathbf{r}}$ (magnitudes r) is the vectors from dA to the center of curvature of the wavefront (the geometrical focus, or the point of minimum confusion) $\underline{\mathbf{s}}$ (magnitudes s) is the vectors from dA to the point of the calculated PSF, $\underline{\mathbf{p}}$, $\underline{\mathbf{n}}\hat{}\underline{\mathbf{r}}$ $\underline{\mathbf{n}}\hat{}\underline{\mathbf{s}}$ are the angles between $\underline{\mathbf{n}}$ and the vectors $\underline{\mathbf{r}}$ and $\underline{\mathbf{s}}$

Approximation fail for large apertures and short focal lengths.

Fresnel-Kirchhoff diffraction integral

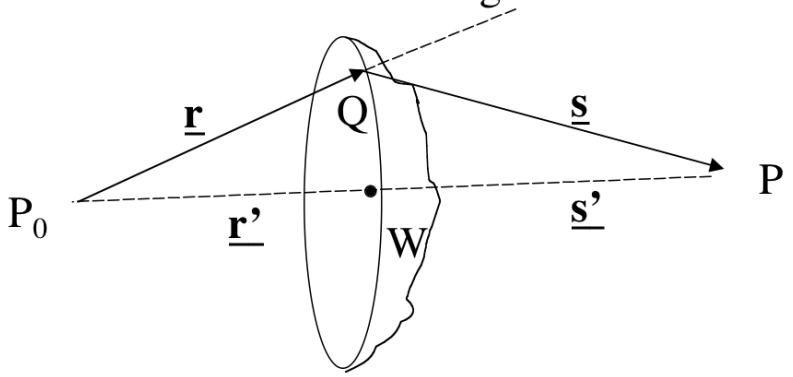

Methods of modeling the microscope PSF

C. SCALAR AND VECTOR MODELS

At high angles need to add VECTOR amplitudes (vertical polarizations do not interfere)
Theoretical models are complex and rely on approximations
Ray Tracing can compute rigorous models at far field only (no apertue effects)

Can show that ray tracing + Kirchhof-Fraunhoffer diffraction integral == FFT(pupil)

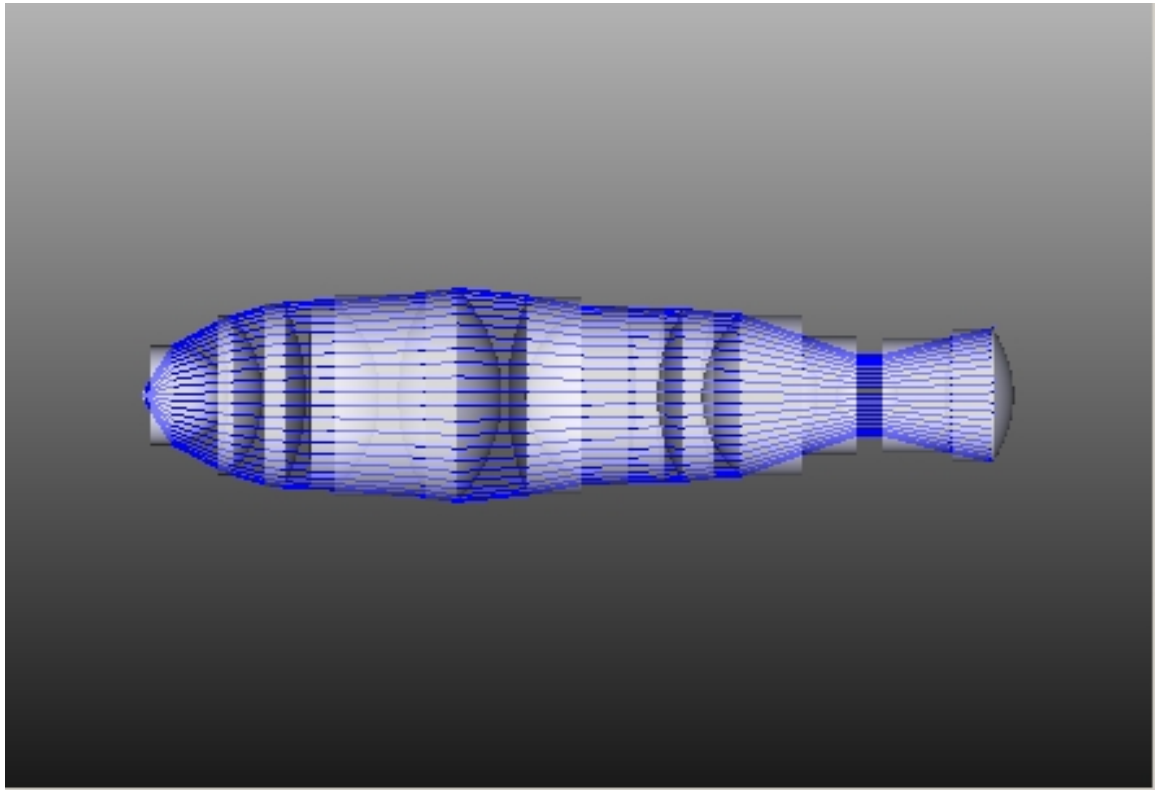

Methods of modeling the microscope PSF

E. 3D FOURIER TRANSFORM OF THE CONVERGING SPHERE

For well corrected microscope $[\cos(\underline{n}\hat{}\underline{r})-\cos(\underline{n}\hat{}\underline{s})] \approx 2$;

$\theta_{max} = \sin^{-1}(NA/n)$

$$\mathbf{PSF(\underline{s}) = | \int E(K) \exp[i\, \underline{k}.\, \underline{s}]\, \delta(k-k_0)\, d^3k\, |^2}$$

$$\int \exp\{i\underline{k}\bullet\underline{r}\}\, d\,(k-k_0)\, d^3k =$$

$$= \int \exp\{i\, k_0\, [x\sin\theta\cos\varphi + y\sin\theta\sin\varphi + z\cos\theta]\}\, k_0^2 \sin\theta\, d\theta\, d\varphi =$$

$$= \int \exp\{i\, k_0 \sin\theta\, [x\cos\varphi + y\sin\varphi]\}\ \mathbf{\exp\{i\, k_0 z\cos\theta]\}}\, k_0^2 \sin\theta\, d\theta\, d\varphi$$

Stokseth's term

3D -> 2D integration

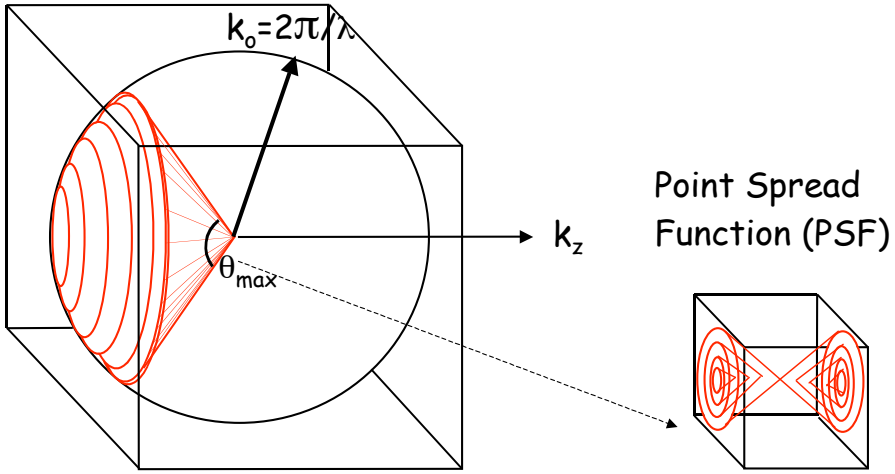

Methods of modeling the microscope PSF

E. 2D FOURIER TRANSFORM OF THE BACK-PUPIL

Fast and useful, since pupil intensities (and phases) can be measured

$$PSF(\underline{s}) = \left| \int E(K) \exp[i\, \underline{k}.\, \underline{s}]\ \exp\{i\, k_0 z \cos\theta]\ d^2k \right|^2$$

Stokseth's two dimensional FFT of the defocus PSF

Stokseth, P.A. (1969) Properties of a defocused optical system. J. Opt. Soc. Am. 59:1314-1321.

Approximation [Eq. 18] $\omega=z(1-\cos a)$ $\alpha<<1$ $z\sim\lambda$ small defocusing & small angle

[Eq. 17] $\omega=1/2\, z\alpha^2[1-z/(r+z)]$ $\alpha<<1$ f/>>1 f-number ==f/ = 1/(2 tana)

precise relation [Eq. 14] $\omega= -r -z\cos\alpha +\sqrt{r^2+2rz+z^2\cos^2\alpha}$

defocused puplil function [Eq. 3] $\exp\{i\, k\, \omega\}$

$\underline{K}= (K_x, K_y) = K(\cos\varphi, \sin\varphi)$

$|\partial^2\underline{K}_{xy}/\partial^2 K\varphi| = K \begin{vmatrix} \cos\varphi & \sin\varphi \\ -\sin\varphi & \cos\varphi \end{vmatrix} = K \quad d^2K == dK_x dK_y = K\, dK\, d\varphi$

$|\underline{K}| \equiv K= k_0\sin\theta \qquad \underline{K} = k_0\sin\theta\,(\cos\varphi, \sin\varphi)$

$|\partial^2\underline{K}_{xy}/\partial^2\theta\varphi| = k_0^2 \begin{vmatrix} \cos\theta\cos\varphi & \cos\theta\sin\varphi \\ -\sin\theta\sin\varphi & \sin\theta\cos\varphi \end{vmatrix} = k_0^2\sin\theta\cos\theta$

$PSF(R,z) = |\int \exp\{i\underline{K}\bullet\underline{R}\}\exp\{i\, k_0 z\,(1-\cos\theta)\}\, d^2K|^2 =$

$=|\int\exp\{i\, k_0 \sin\theta\,[x\cos\varphi+y\sin\varphi]\}\exp\{ik_0 z(1-\cos\theta)]\}k_0^2\sin\theta\cos\theta d\theta d\varphi|^2$

for a general aberrated pupil function, Pupil(θ, φ)

$PSF(R,z) =| \int \text{Pupil}(\theta,j)\exp\{i\underline{K}\bullet\underline{R}\}\exp\{i\, k_0 z\,(1-\cos\theta)\}\, d^2K|^2=$

$\equiv| \int \text{Pupil}(\theta,\varphi)\exp\{i\underline{K}\bullet\underline{R}\}\,\text{Defocus}(\theta,z)\, d^2K|^2$

$\text{Defocus}(\theta,z) \equiv \exp\{i\, k_0 z\,(1-\cos\theta)\}$

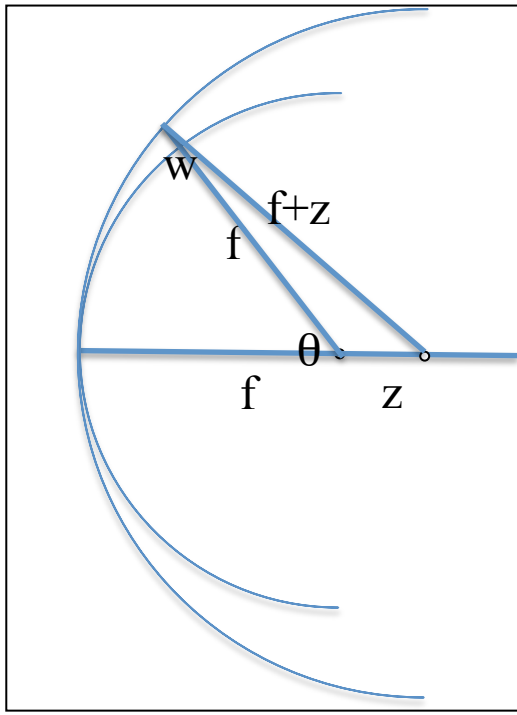

$w= f+z-\sqrt{f^2+2fz+z^2\cos^2\theta} \sim z(1-\cos\theta)$

For the "field corrected" microscope obeying Abbe's sine condition

$\sin\theta/\sin\theta' = \text{const} \qquad h/\sin\theta' = \text{const}$

$|\text{Pupil}(\theta,\varphi)| = (\cos\theta)^{-1/2}$

Depth Aberration

For depth-aberration

$PSF(R,z) = \equiv |\int \text{Pupil}(\theta, \varphi) \exp\{i\underline{K}\bullet\underline{R}\} \text{Defocus}(\theta,z) \text{Depth}(\theta,d)\ d^2K|^2$

$\text{Pupil}(\theta, \varphi)=(\cos\theta)^{-1/2}\ \text{Depth}(\theta,d)$

(a) $\text{Depth}(\theta,d) \equiv \exp(ik_0 d[n'\cos\theta' - n\cos\theta])$

(b) $\text{Depth}(\theta,d) \equiv \exp(ik_0 d[n'\cos\theta'])$

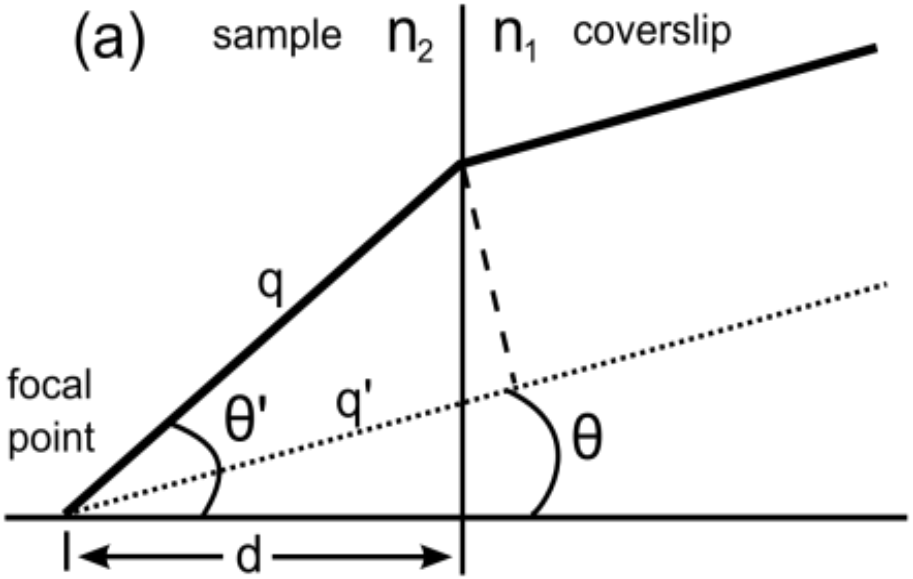

Correction of the depth aberration

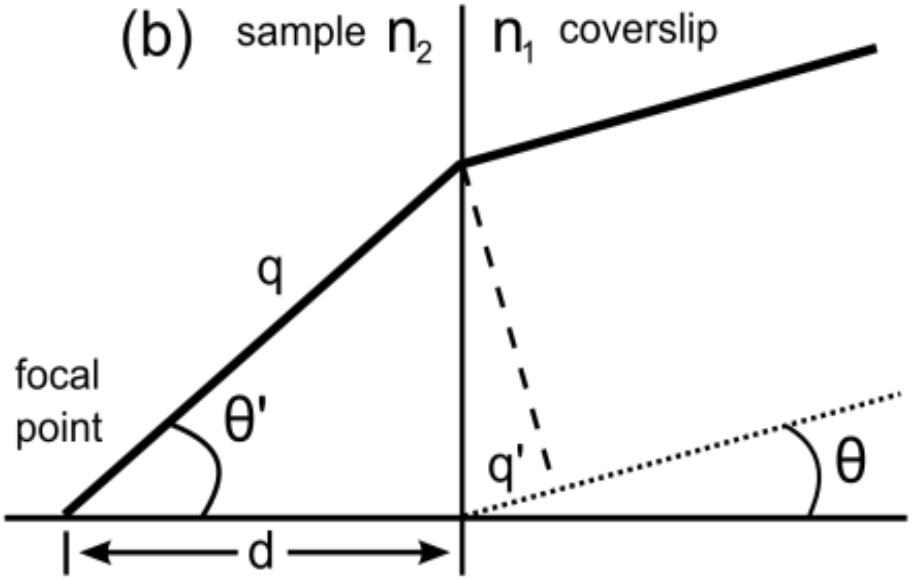

Focusing and correction of aberrations

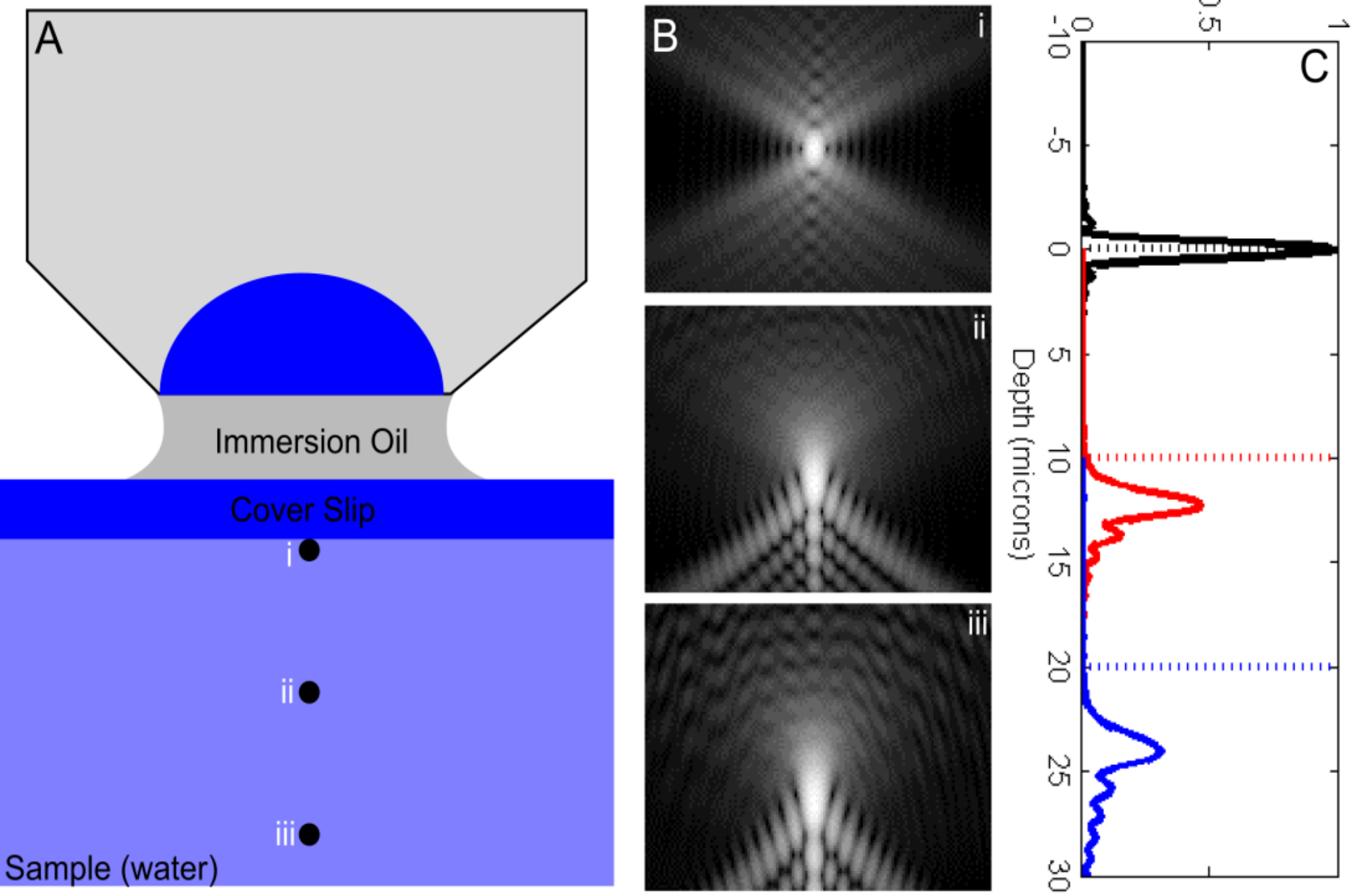

Effect of depth aberrations on microscope point-spread function (PSF).

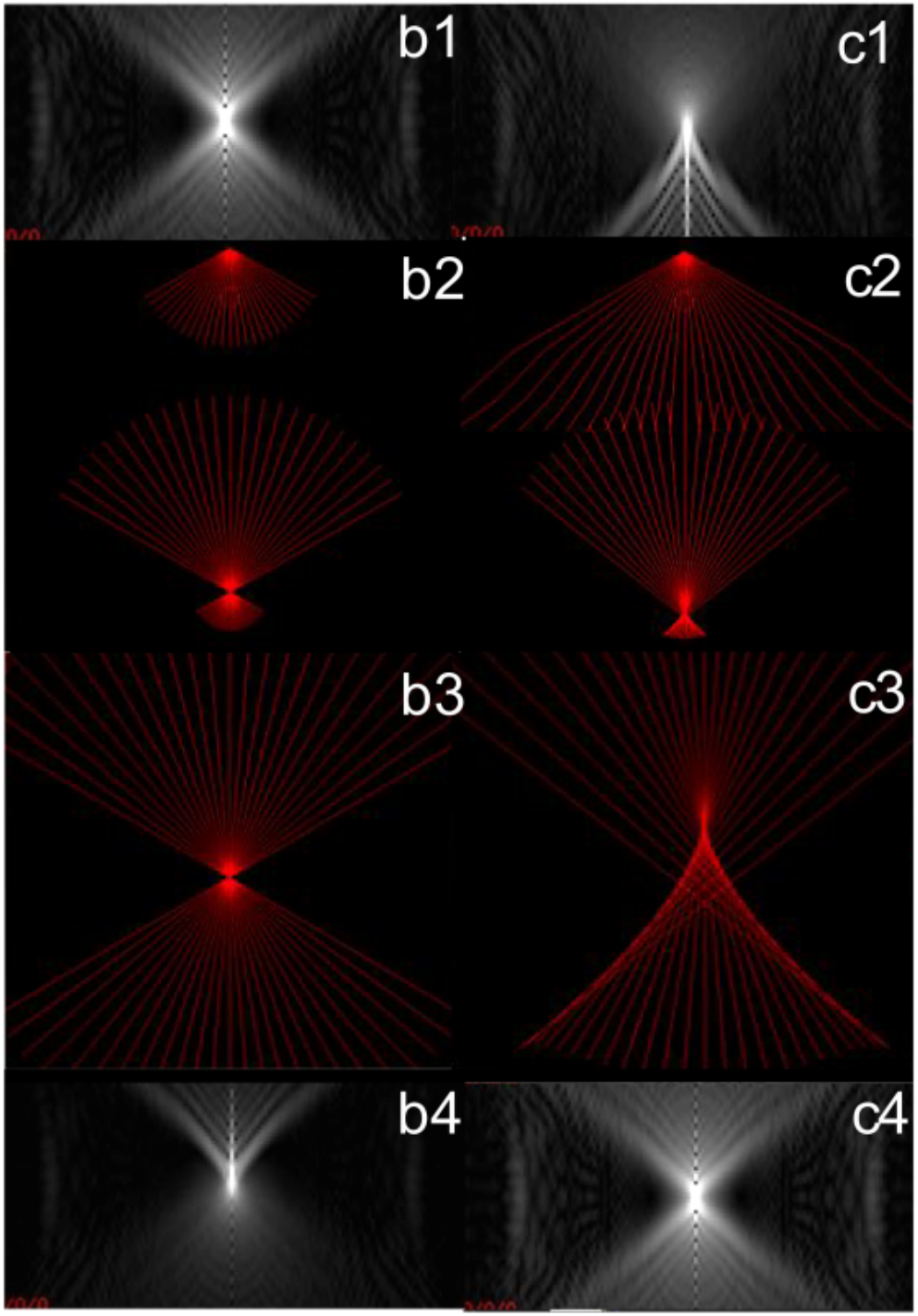

(b1) Calculated PSF of an ideal microscope. (b2) plotted ray paths emerging from a point Under the microscope (bottom fan) and exiting the microscope to focus at the image plane (top fan of rays). (b3) Enlarged view of rays converging onto the focal point. (c1) The PSF computed with a layer of water in the imaging path showing the typical spherical aberration. (c2) The geometrical optics pattern due to refraction in a layer with refractive index different from the immersion Oil (depicted in the top ray fan). (c3) Enlarged view of (c2) near the focus, with the Geometrical optics pattern corresponding to the aberrated PSF of (c1). (b4) The PSF computed for the ideal microscope optics in which the adaptive element introduces the phase corrections according to Eqn. (1) for the layer of water. The PSF shows a spherical aberration 'inverted' to that in (c1). (c4) The PSF for imaging into water with phases corrected by the adaptive element, showing The recovery of the non-aberrated PSF. (Kam et al., 2007)

AO CORRECTION OF DEPTH ABERRATION

1. Accurately model 3D PSF by ray tracing and pupil integration
2. Know to predict the phase correction for “depth aberration”
3. Use AO to introduce this phase into the optical system at the pupil plane conjugate
4. We can also introduce a spherical phase that will shift the focal plane

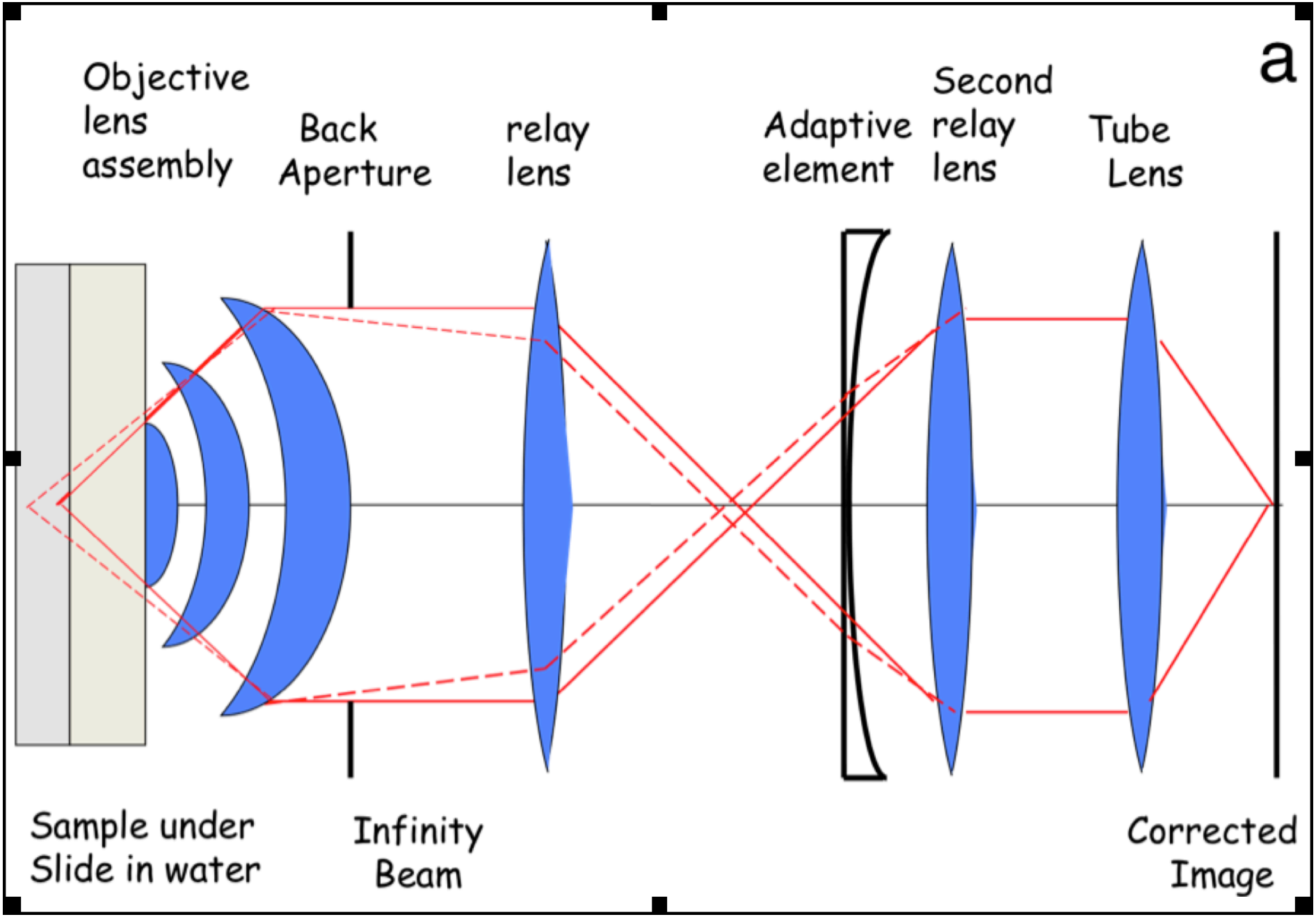
a
Objective lens assembly
Back Aperture
relay lens
Adaptive element
Second relay lens
Tube Lens
Sample under Slide in water
Infinity Beam
Corrected Image

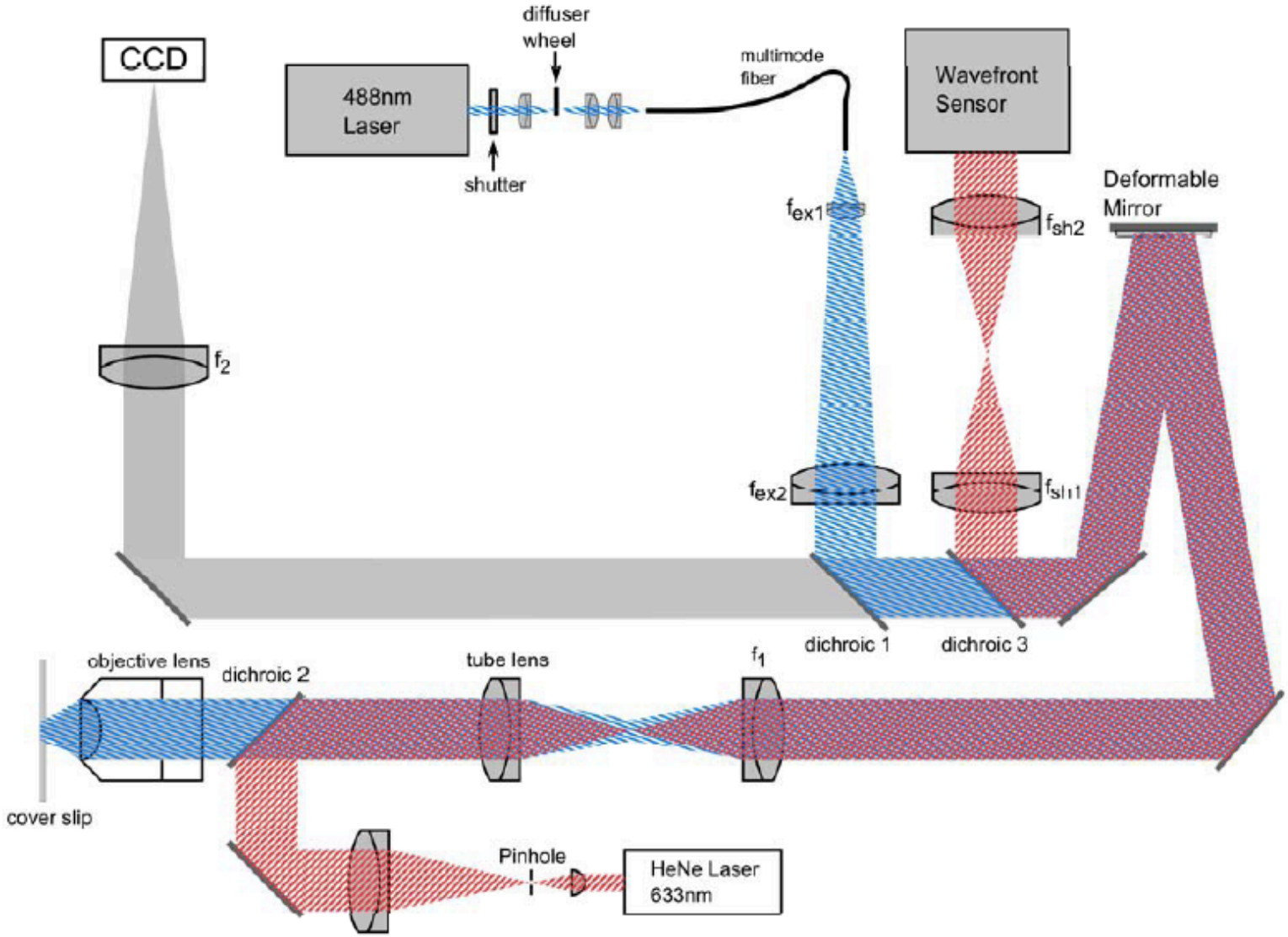

AO Microscope Layout

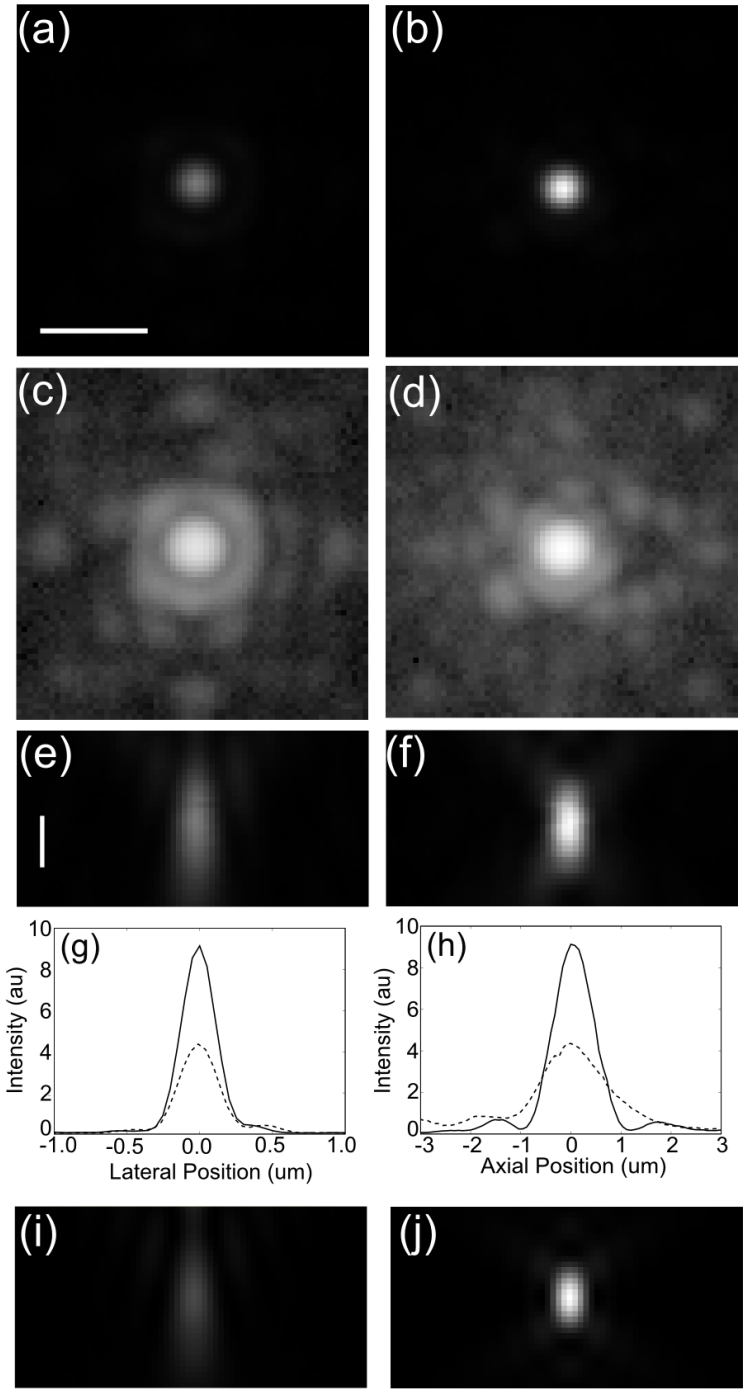

Depth aberration correction: beads gain intensity

Images of a 200nm bead 67µm below the coverslip in a water/glycerol mixture with n=1.42. (a) uncorrected image of in-focus plane. (b) corrected image of in-focus plane: same scale as (a). (c) and (d) are the same as (a) and (b) respectively but on a logarithmic scale. (e) and (f) are cross-sections through the focal plane on a linear scale. The scale bars are 1µm. (g) and (h) are line Profiles of the intensity through the center of the bead along a lateral and the longitudinal axis respectively. The dashed line is from the uncorrected image and the solid line is from the corrected image. (i) and (j) are simulations of the PSF. (i) corresponds to the uncorrected PSF 65 microns into a material with index 1.42 using a 1.2NA objective with a 1.512 refractive index immersion oil. (j) is a simulated PSF at the coverslip. The peak intensity for (j) is 3.75 times the peak intensity for (i).

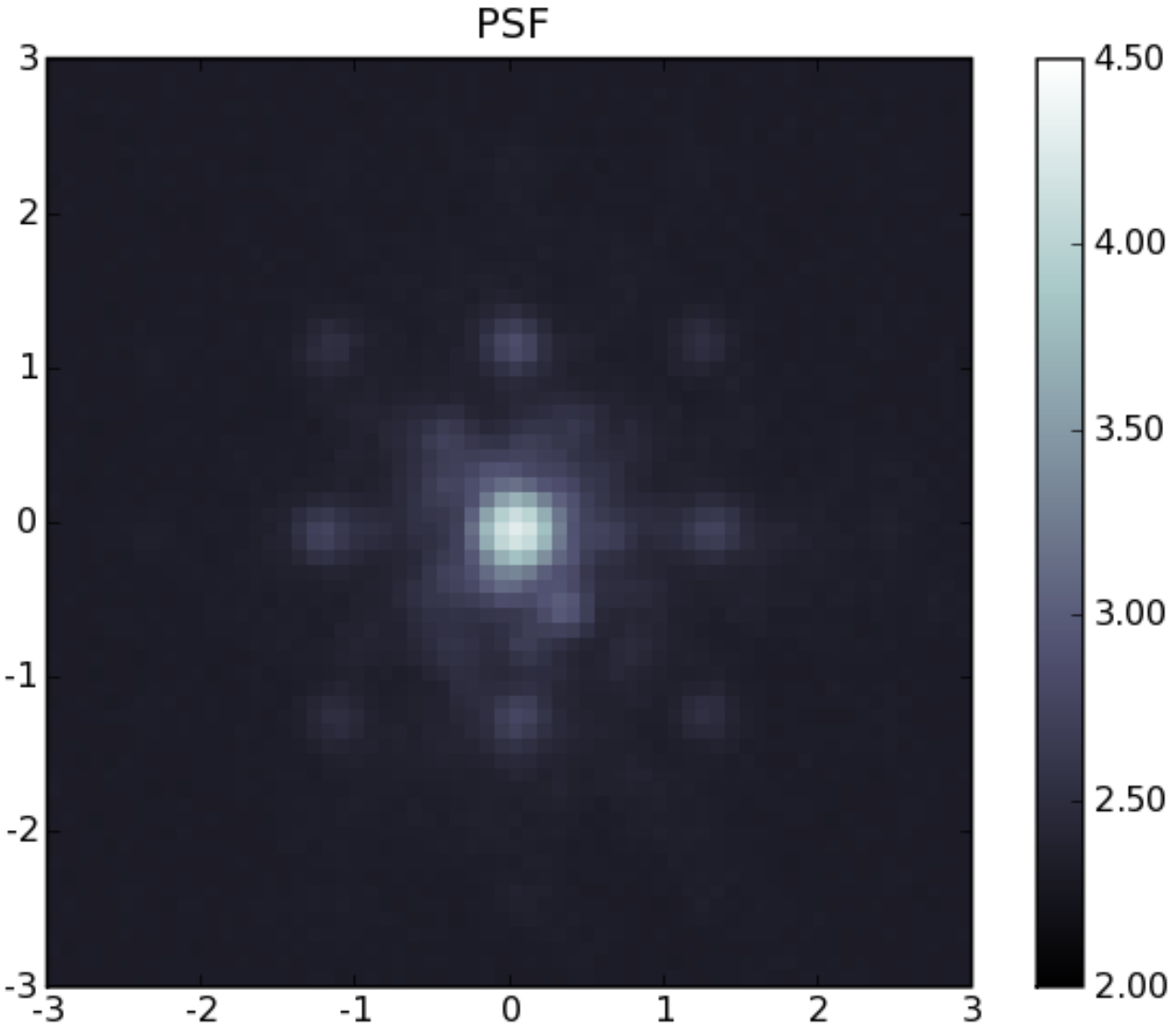

Depth aberration correction: print through effect

Image of a 200nm Yellow-Green Fluorescent bead on a logarithmic scale. Satellite peaks caused by the print-through of the mirror are visible. The maximum intensity of the satellite peaks is ~1% of the central peak, integrated intensity in the satellite peaks reach 10%.

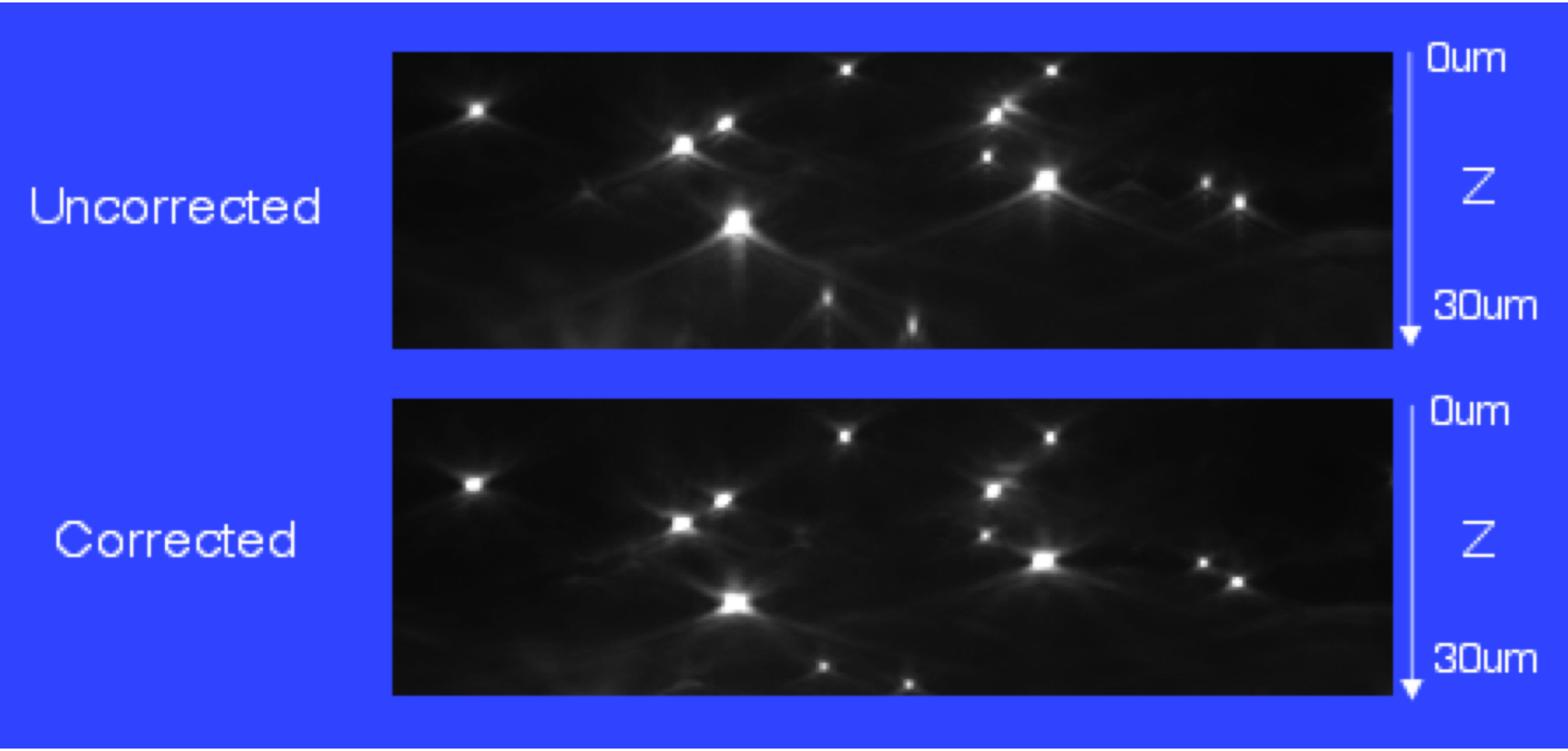
Uncorrected
0um
Z
30um
Corrected
0um
Z
30um

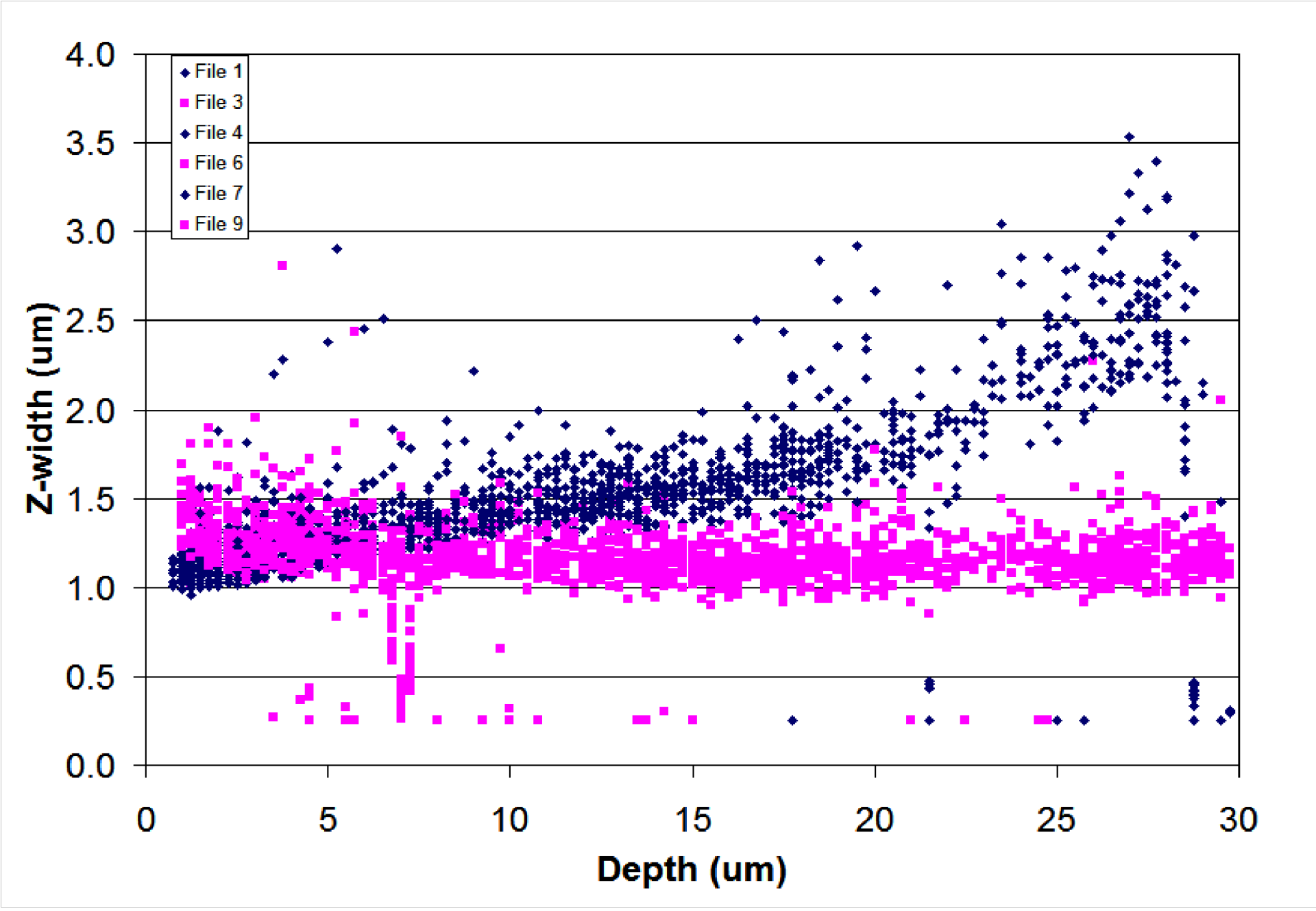
File 1
File 3
File 4
File 6
File 7
File 9
Z-width (um)
4.0
3.5
3.0
2.5
2.0
1.5
1.0
0.5
0.0
0
5
10
15
20
25
30
Depth (um)

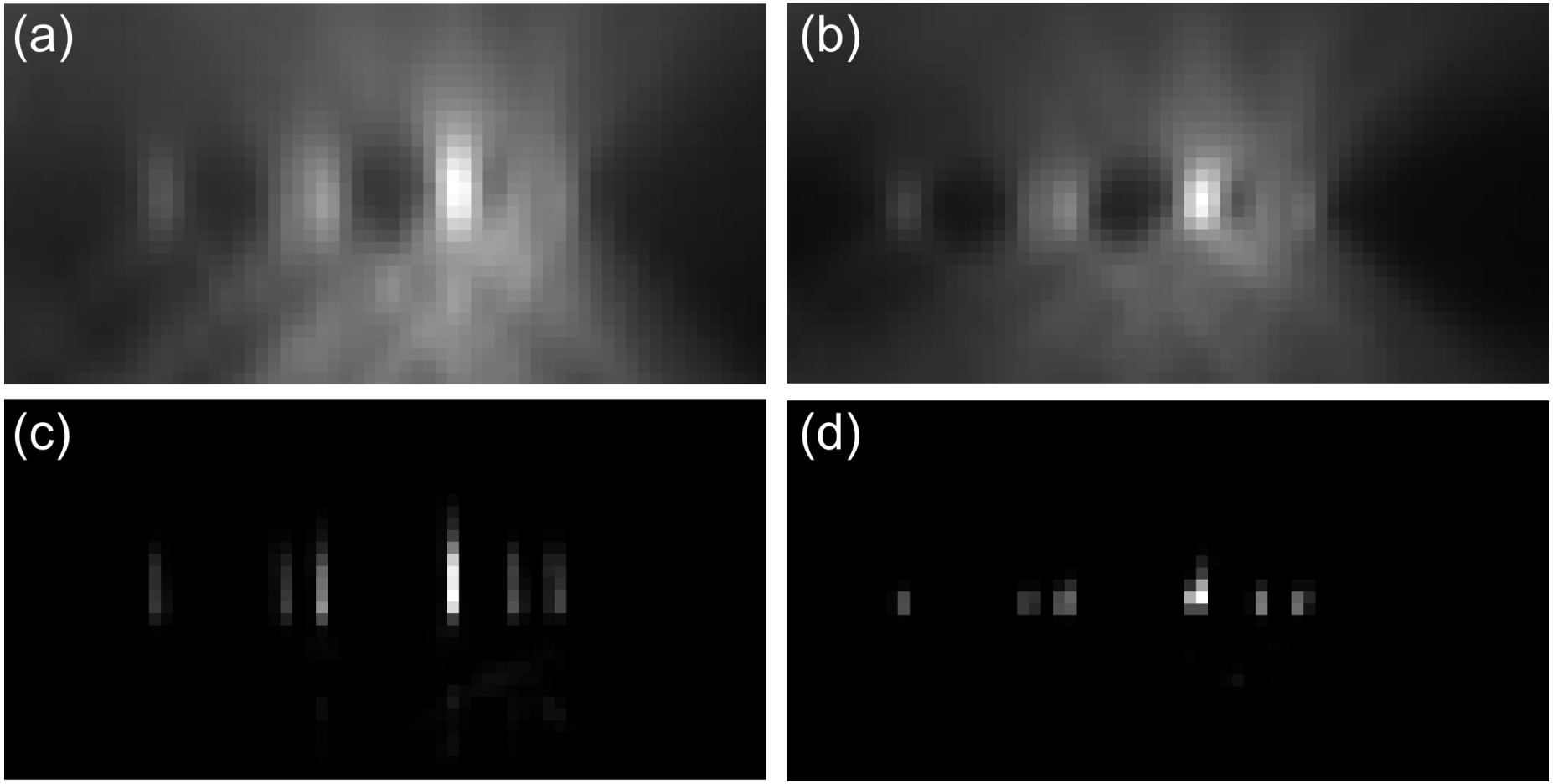

Depth aberration correction: provide space invariant deconvolution

(a) 200nm fluorescent beads in glycerol 64µm below the cover slip imaged with no correction by the DM (b) same beads imaged with the DM set to correct the depth aberration (c) Deconvolution of the image (a) using a PSF measured at the cover slip (d) Deconvolution of the image (b). Each image is independently scaled to its maximum intensity. Each image is 6.0µm in the lateral dimension and 6.4µm in the axial dimension.

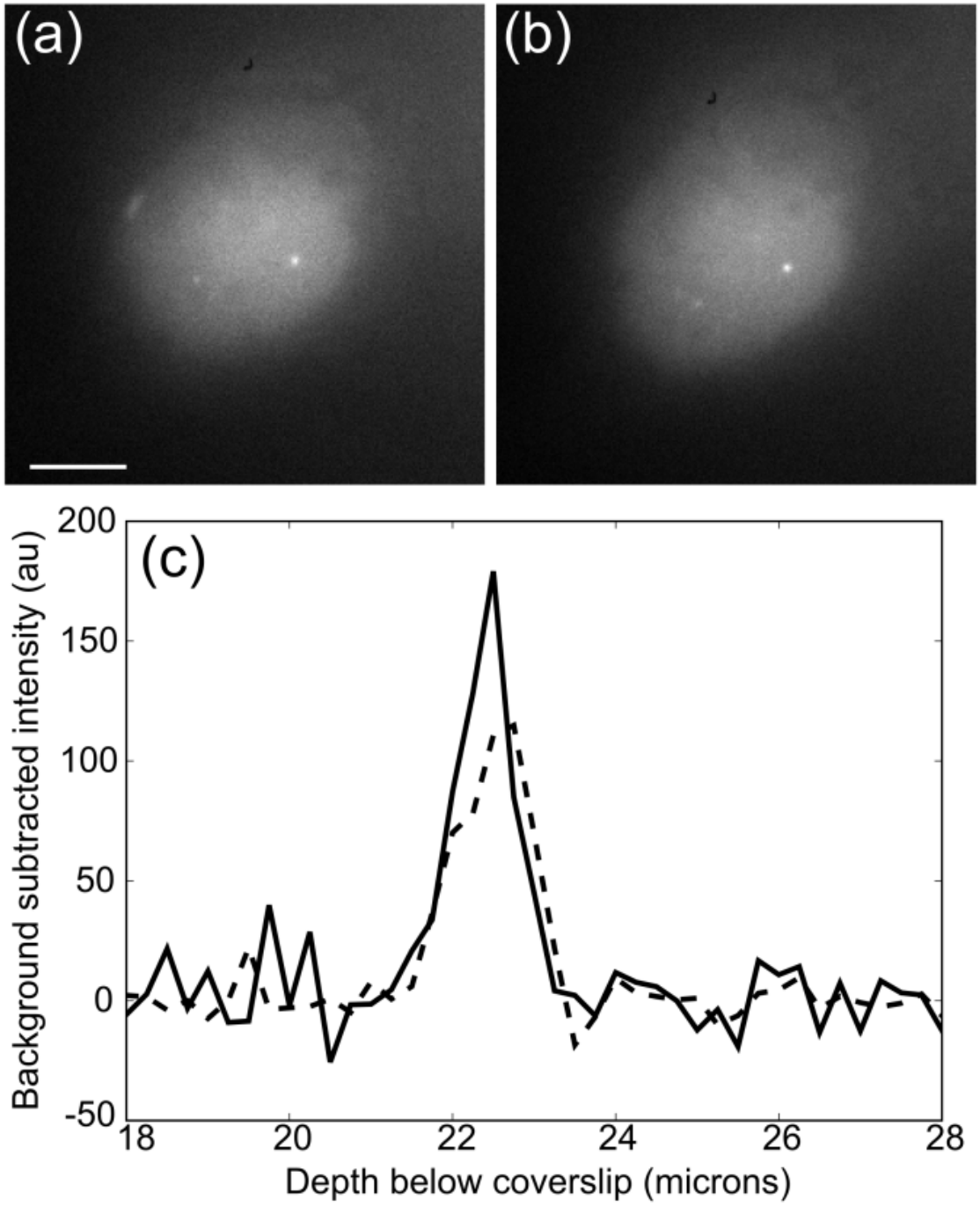

Depth aberration correction
In the nucleus

Images of GFP-TRF1 labeled telomeres in UMUC bladder cancer cells. (a) uncorrected images 23µm below the coverslip. (b) depth aberration corrected 23µm below the coverslip. The correction assumed a sample index of 1.38 (c) Background subtracted profiles through the labeled telomere (bright spot in images a and b) along the axial direction. The line with brown squares is from the uncorrected image a, and the line with blue diamonds is from the corrected image b. The peak intensity in the corrected image is 60% larger over the background. The scale bar is 5µm.

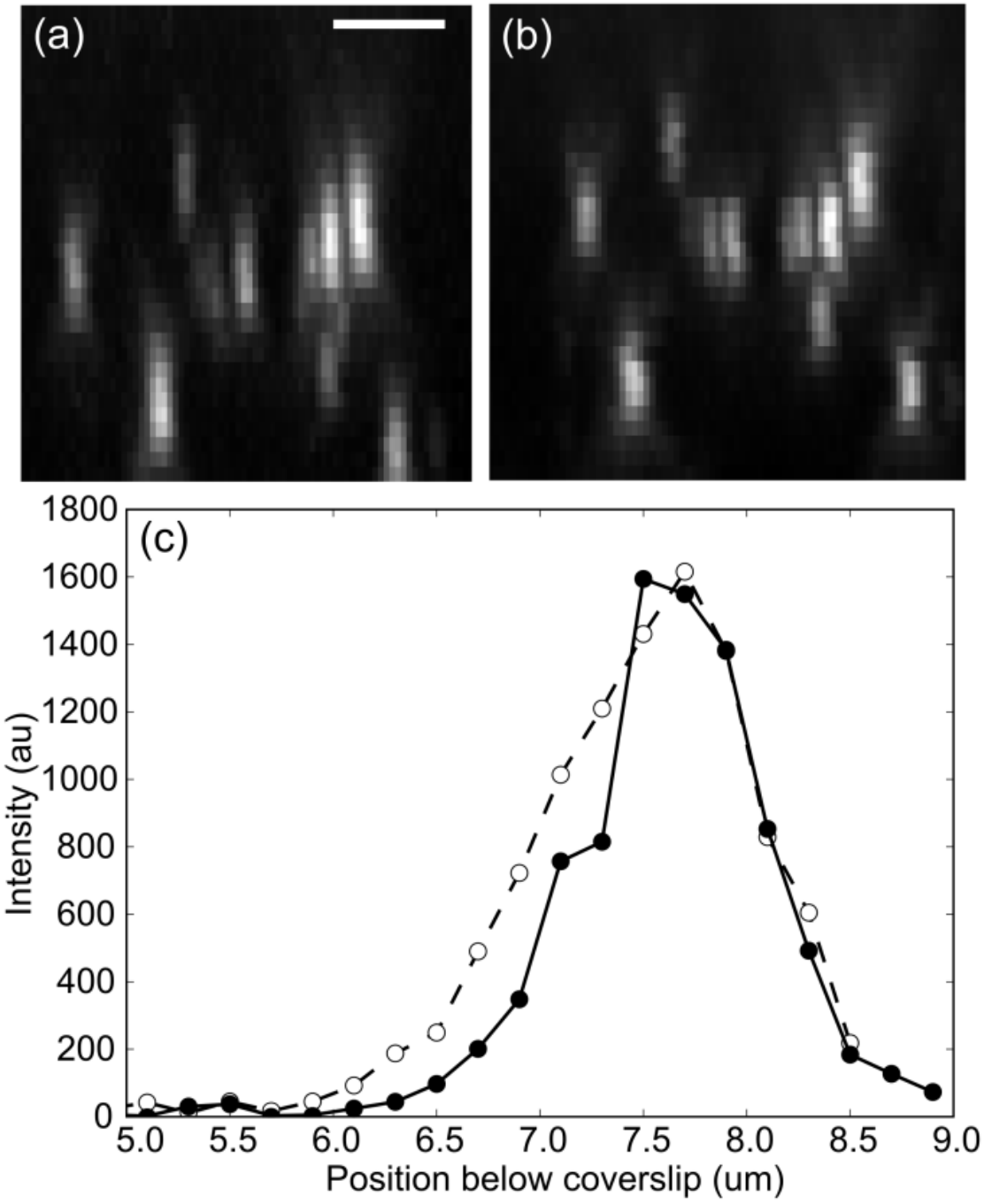

Depth aberration correction In drosophila embryo

GFP labeled centromeres in eye Imaginal Discs in Drosophila embryos. Scale bar is 2µm. (a) Maximum intensity projection of uncorrected three-dimensional data stack. Vertical is the axial direction. The top of the image is 2µm below the coverslip and the bottom is 9µm below the coverslip. (b) Maximum intensity projection of a depth aberration corrected data stack. The correction assumed a sample index of 1.38. (c) Line profiles along the axial direction for uncorrected (filled circles) and corrected (open circles) images of a GFP labeled centromere.

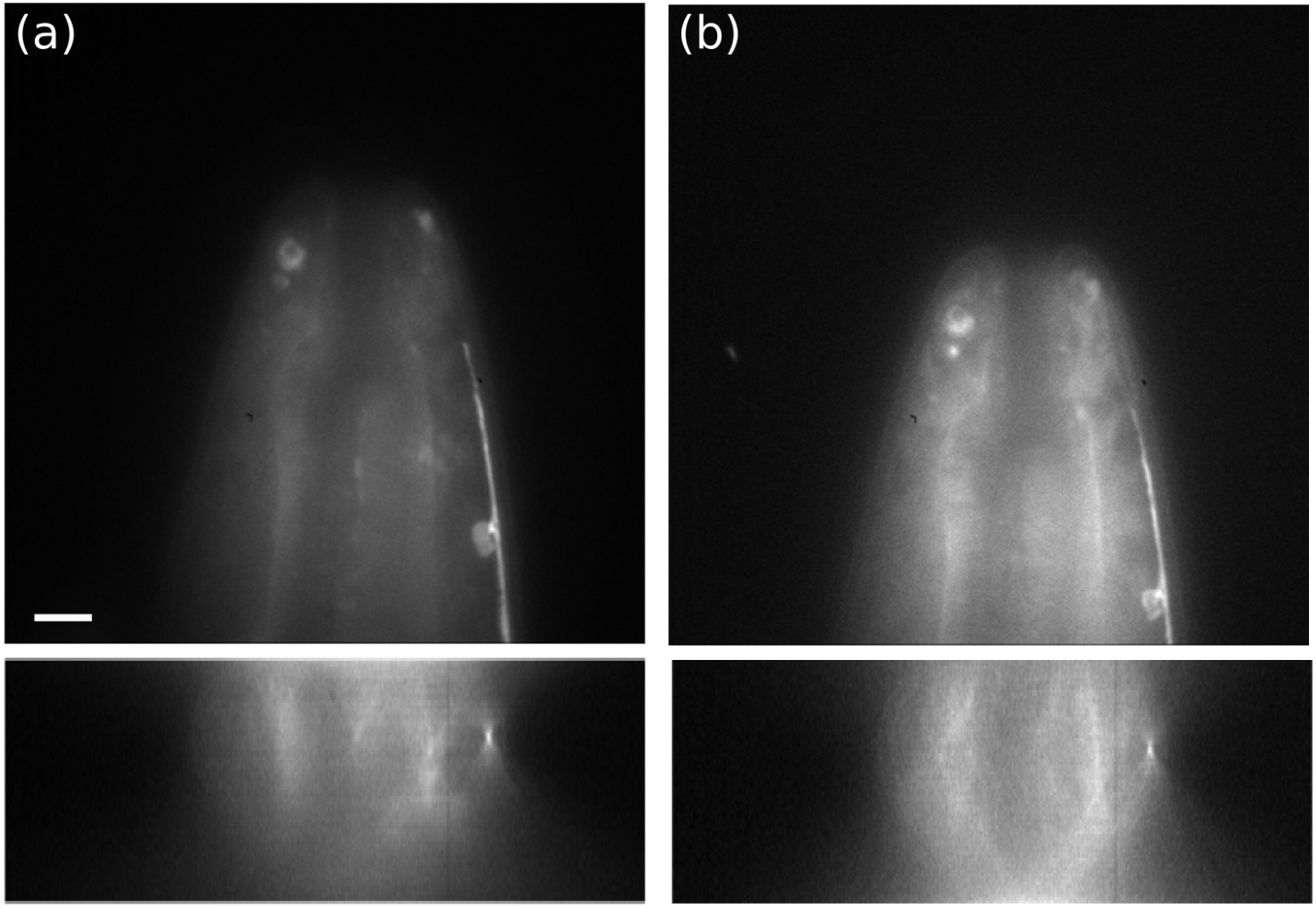

Depth aberration correction in C. elegans

Comparison of images taken by focusing with the deformable mirror (a) and mechanical focusing (b). Images are of C. elegans expressing a GFP sur-5 construct; the bright feature along the right side is the ventral nerve cord. The top images are taken 6µm below the coverslip and the bottom images are xz cross-sections. The difference in image intensity is due to photobleaching. Each image is scaled to its maximum intensity. A sample refractive index of 1.36 was assumed for focusing with the deformable mirror using equation 2. The scale bar is 2µm.

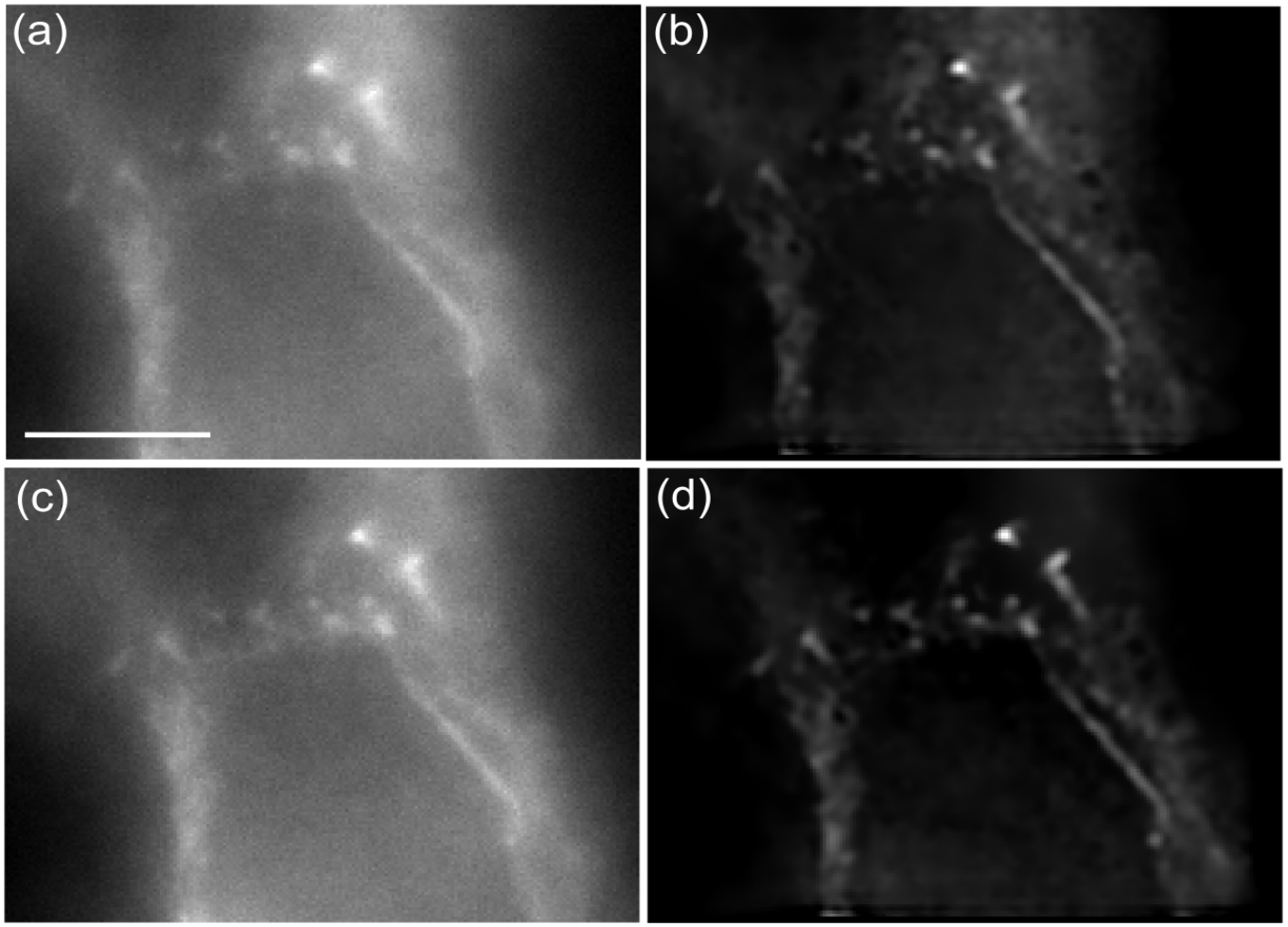

Depth aberration correction and deconvolution for cells:

Deconvolved images of alexa488-phalloidin labeled B16F10 mouse cells. Images are 4.4μm below the coverslip. (a) uncorrected image. (b) uncorrected deconvolved image (c) image corrected by adaptive optics. The correction assumed a refractive index of 1.38 (d) image corrected by adaptive optics after deconvolution. The scale bar is 5μm.

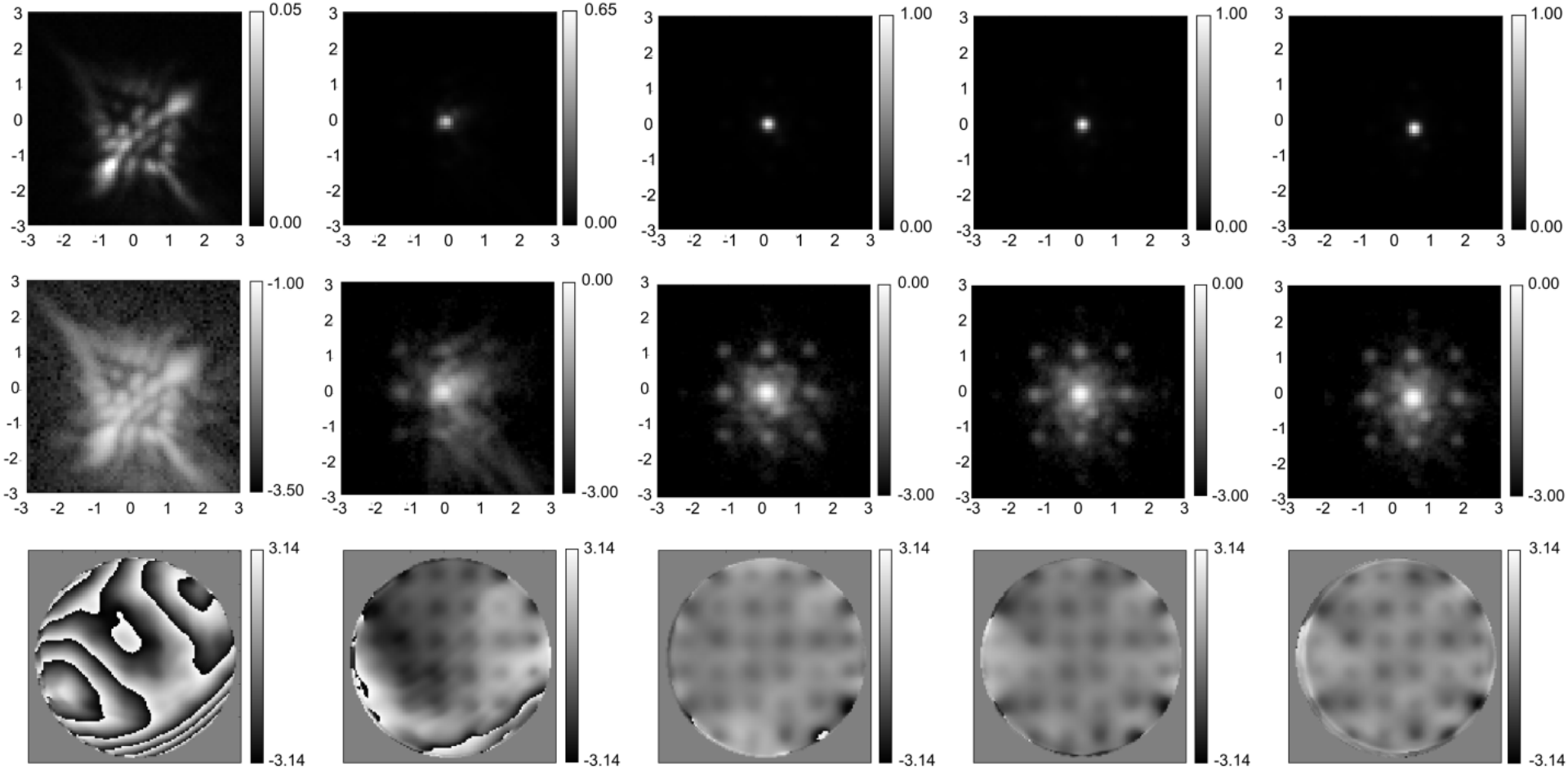

Iterative correction of the microscope point spread function. Top row: In focus image of the PSF, linear scale. Second row: same as first row but on a log scale. Third row: phase in the back pupil plane calculated from phase retrieval with the tip, tilt and focus terms removed. First column: before correction; DM actuators all set to zero volts. Each successive column is after a round of iteration.

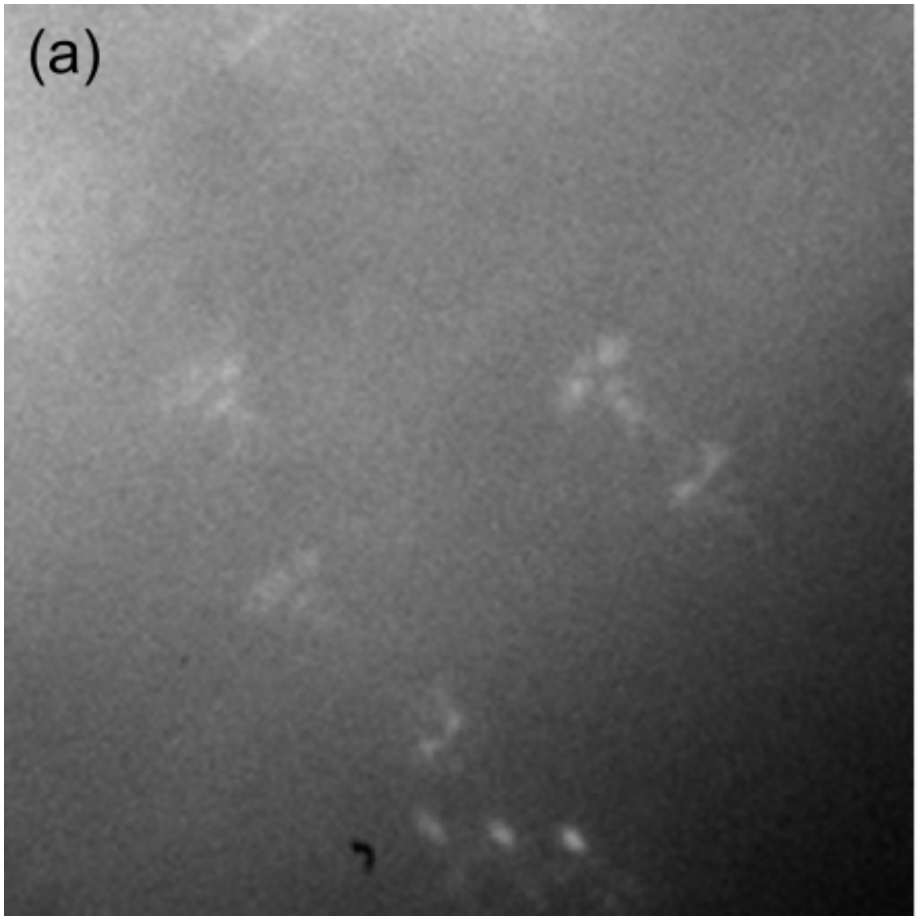

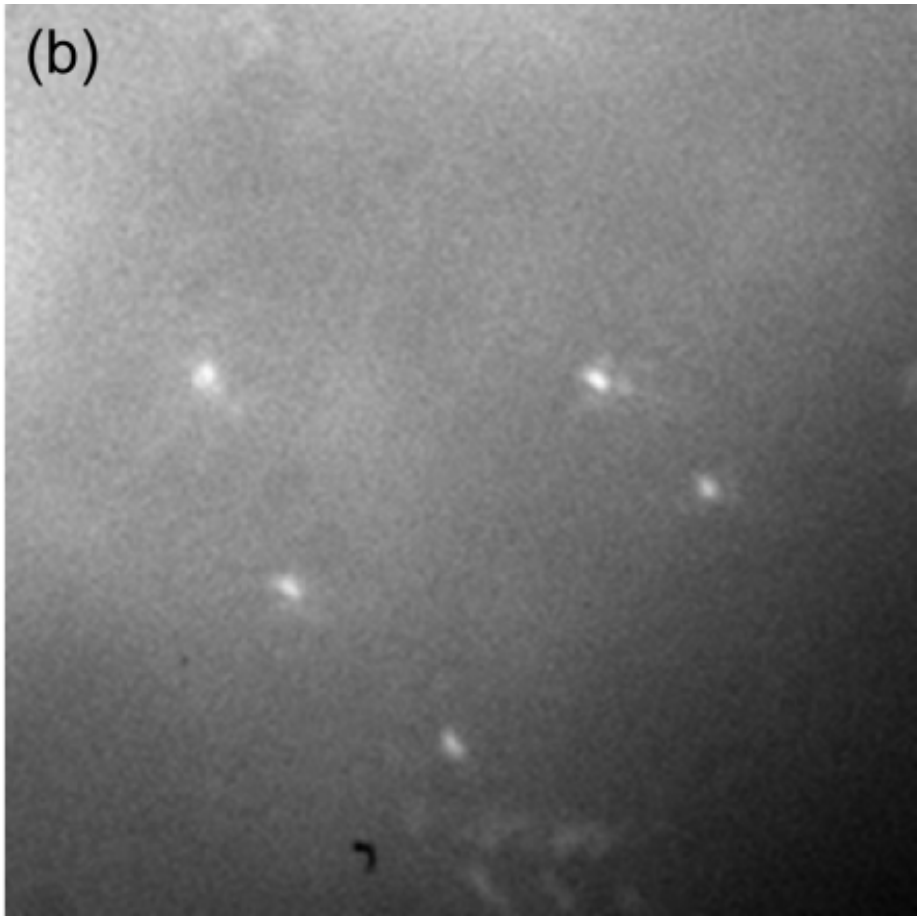

Depth aberration correction with AO optimization by feedback:

Image of 200nm fluorescent beads on a microscope slide below a *C. elegans*. (a) Image taken with a flat DM. (b) Image taken with the DM shape set to optimize the bead intensity using the algorithm described in (Booth, 2006).

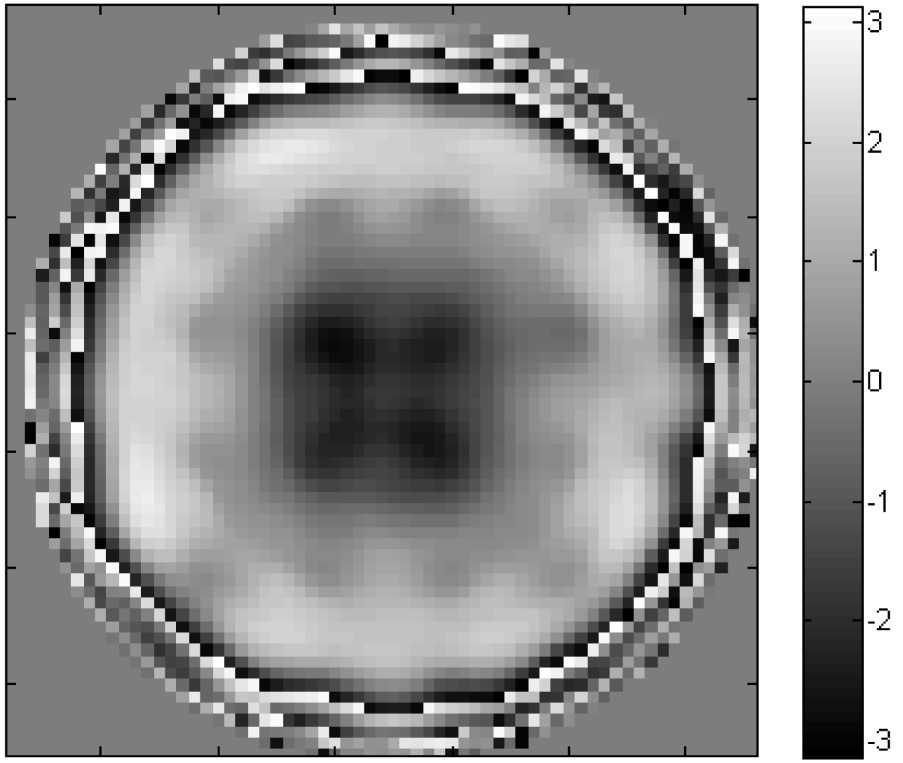

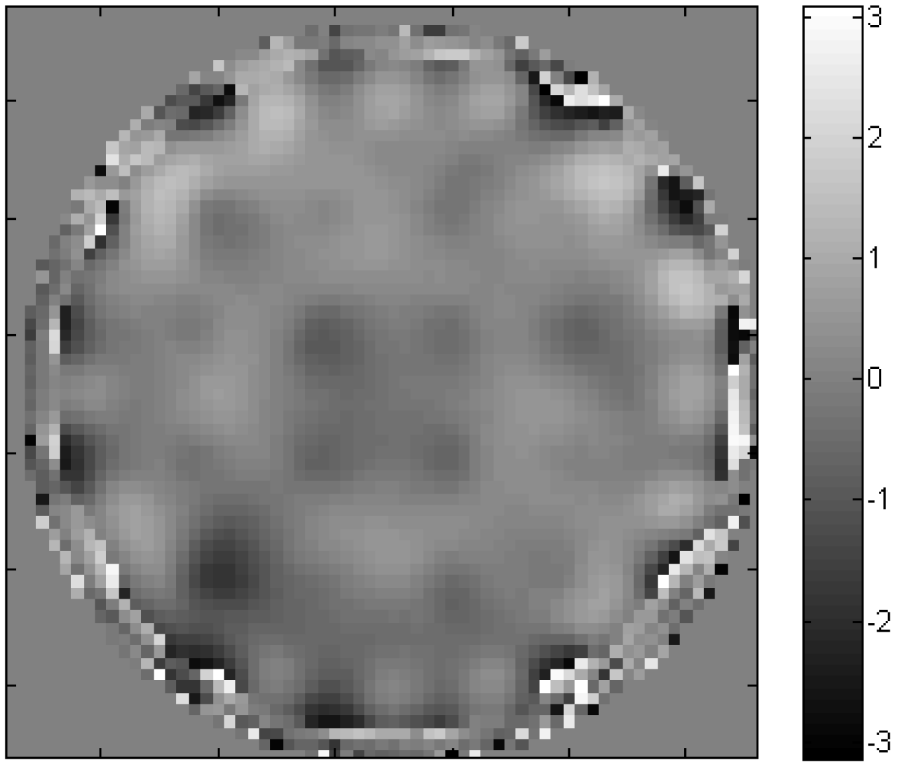

The back aperture:

Phase in back pupil plane calculated by phase retrieval from the uncorrected PSF (left) and the corrected PSF (right).

SUMMARY

Depth aberration has small effect on PSF width at focus,
but large effect on PSF height (Z) and maximum intensity

For sufficiently high S/N the correction does not look dramatic

At lower S/N applications (e.g. for single fluorophore detection in 3D super-resolution microscopy) the correction becomes critical

AO can be applied for motionless focus through 3D sample volume

SAMPLE-INDUCED ABERRATIONS

1. Depth aberration: largest contribution in biological 3D imaging
2. Secondary distortions are from sample-induced aberration
3. Correction is possible in scanning confocals by point-by-point optimization feedback
4. Propose hypothetical correction scheme for wide-field: inverse sample

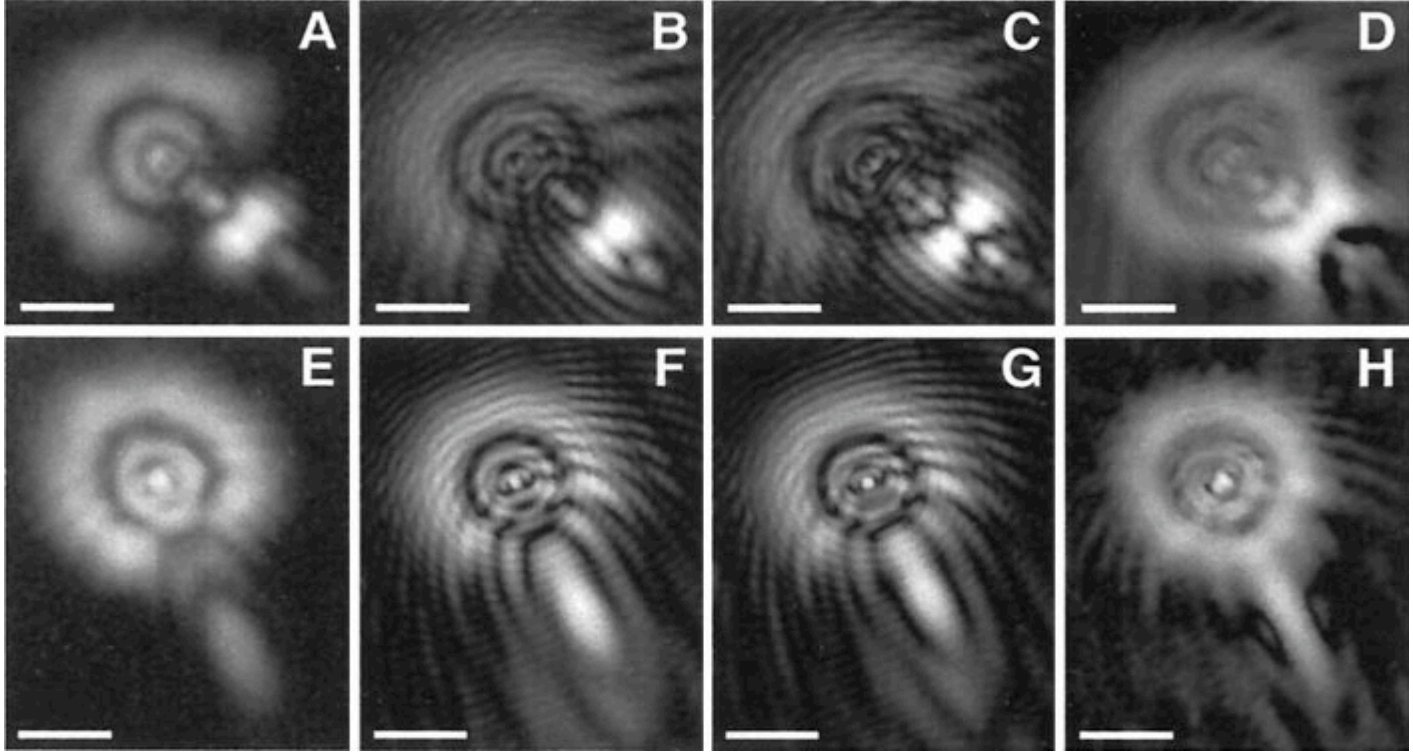

Simulated and measured sample-aberrated PSFs (Kam et al., 2001). Refractive index map of the specimen was retrieved from three-dimensional DIC images using LID Integration (Kam, 1998). A–D are defocused optical sections of a bead aberrated by an oil drop below the cover slip at 3.0μm below focus and E–H are optical sections of another aberrated bead at 2.75μm below focus. (A and E) a measured image of the 0.1μm bead. (B and F) a computed 3D ray-traced PSF using a refractive index map from the line integrated oil drop DIC data. (C and G) a ray-traced PSF using simulation of an oil drop with uniform known refractive index. (D and H) a computed PSF in which the aberrated wavefront calculated by ray tracing through a simulated oil drop of uniform refractive index was applied to a measured, unaberrated PSF. (Scale bars, 2μm.)

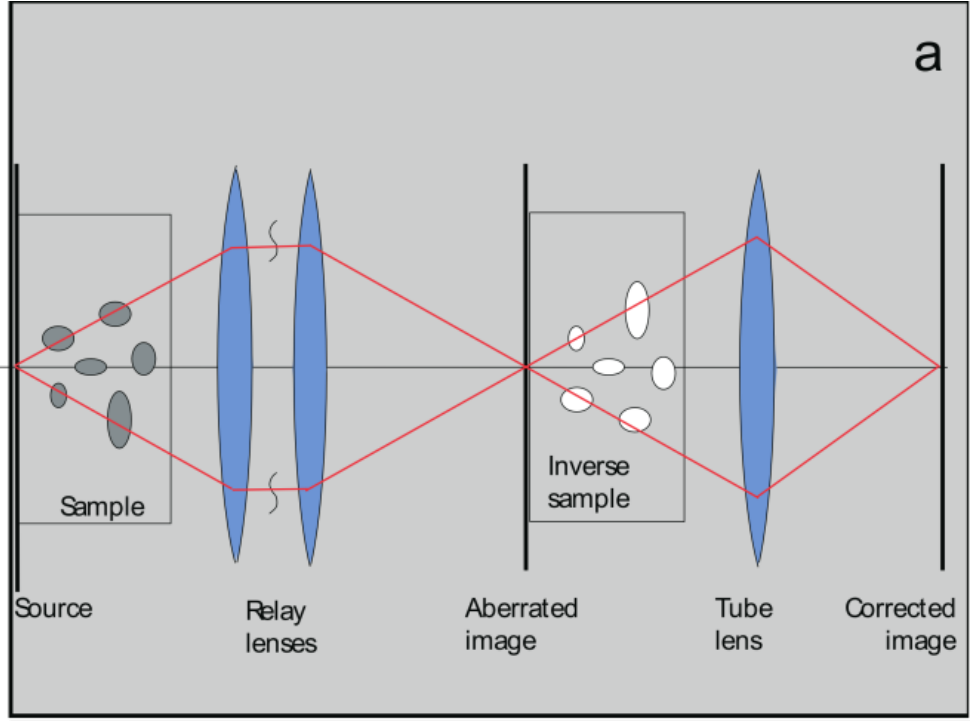

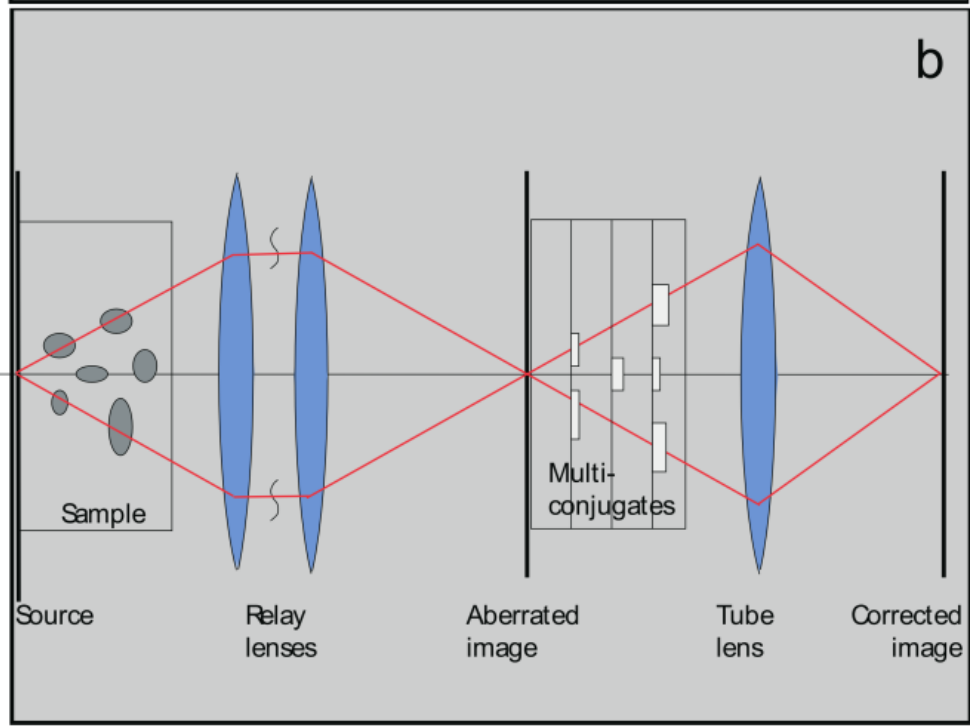

Sample-induced aberration

Schematic optical setup for correcting sample-induced aberrations (Kam et al., 2007). The sample is simulated by a set of ellipsoids with refractive index different from the embedding medium. ray tracing is performed through the sample volume.
(a) the correction is performed by a hypothetical **"inverse sample"** with the identical distribution of ellipsoids but with the opposite refractive index contrast
(b) The inverse sample is approximated by three adaptive elements, shifting the Phases of rays that pass through them.

PROJECTION

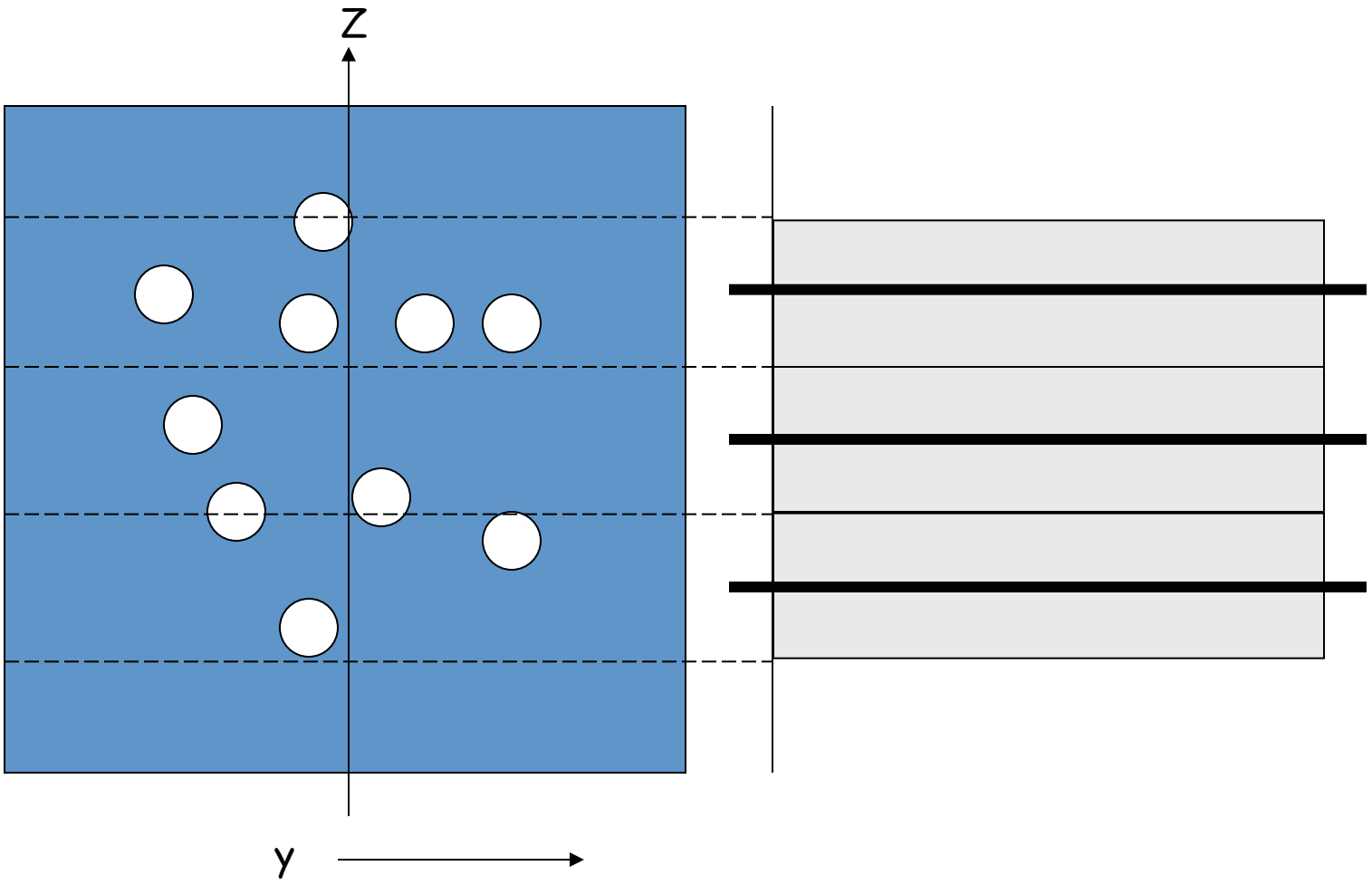

WEIGHTED PROJECTION

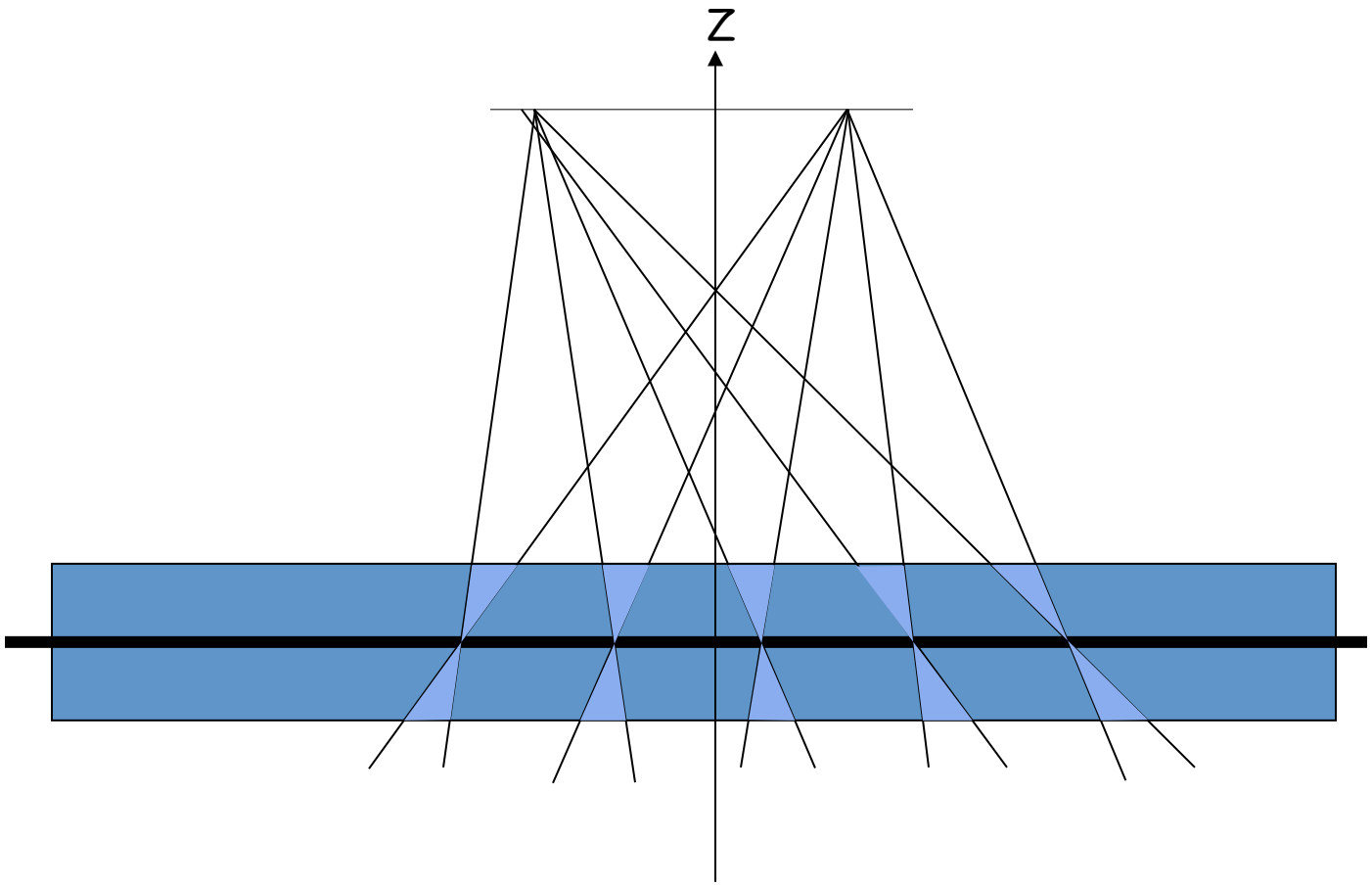

TOKOVININ

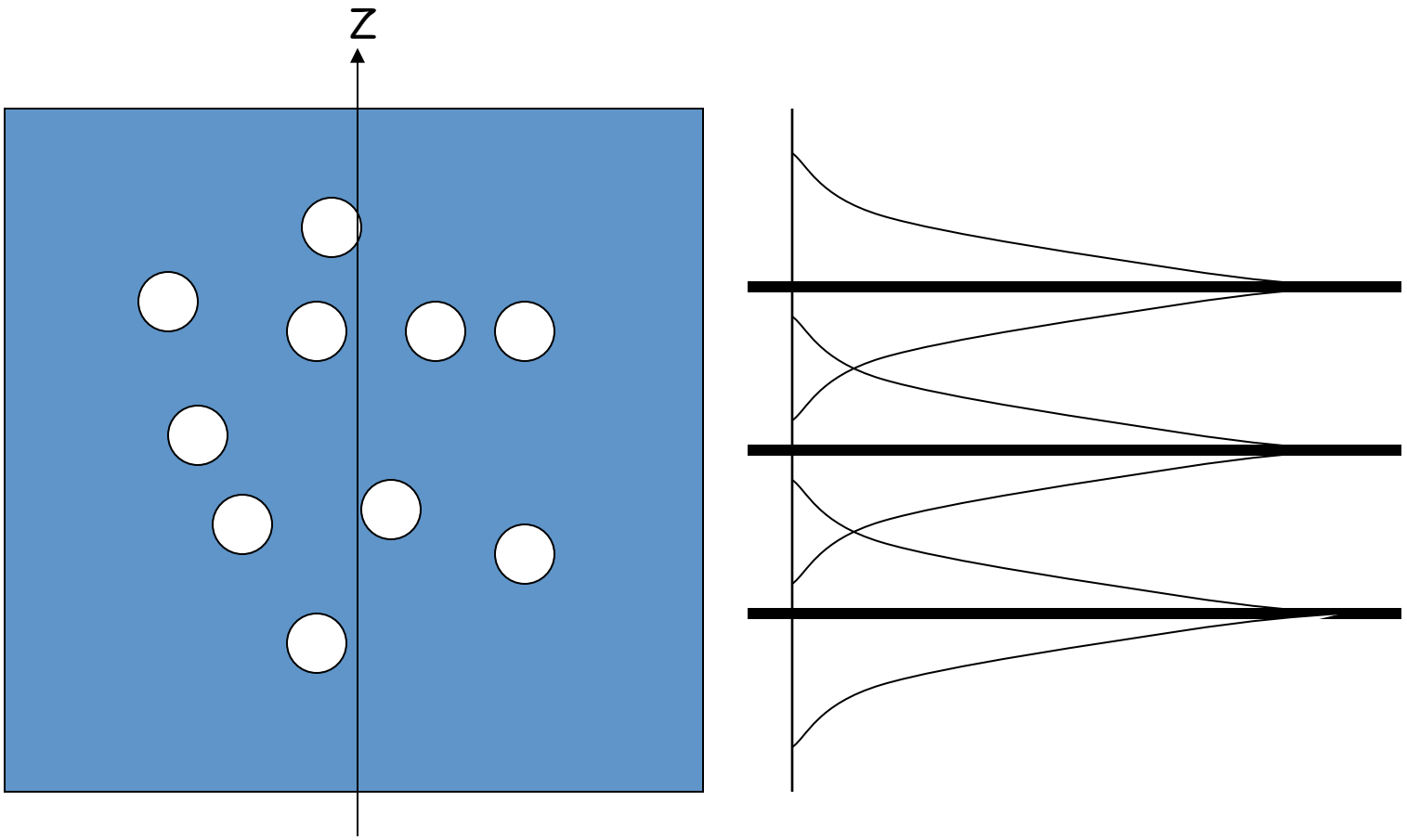

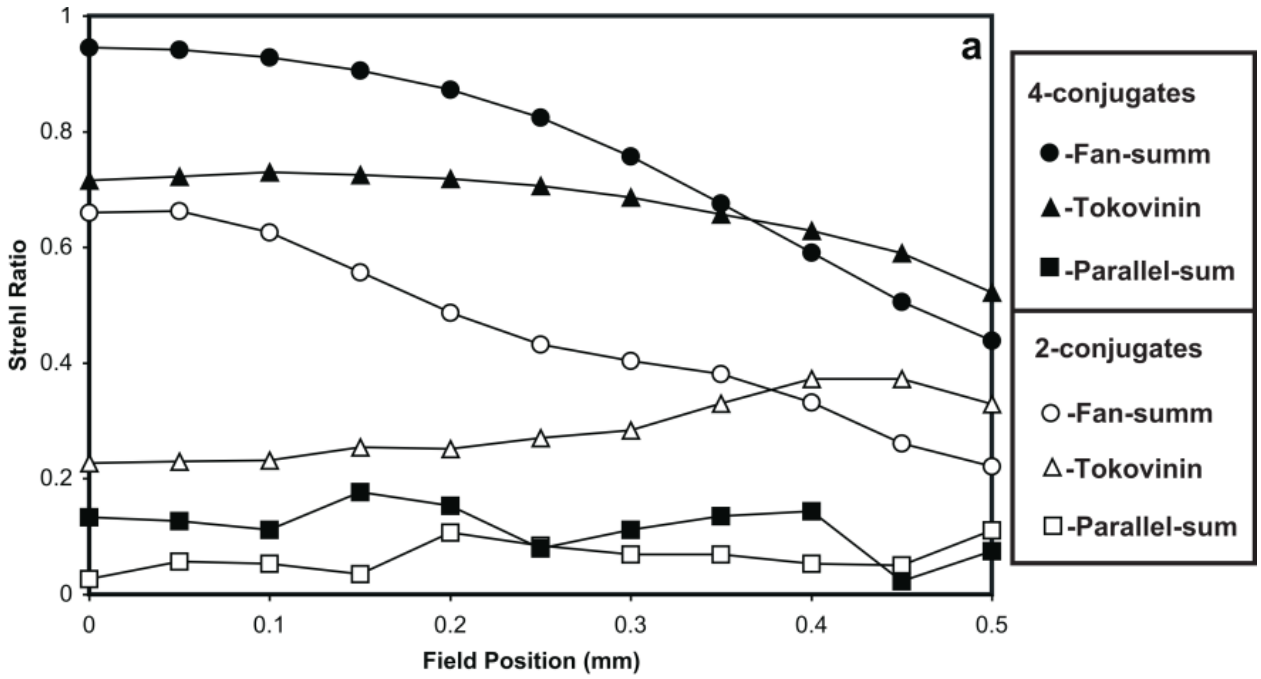

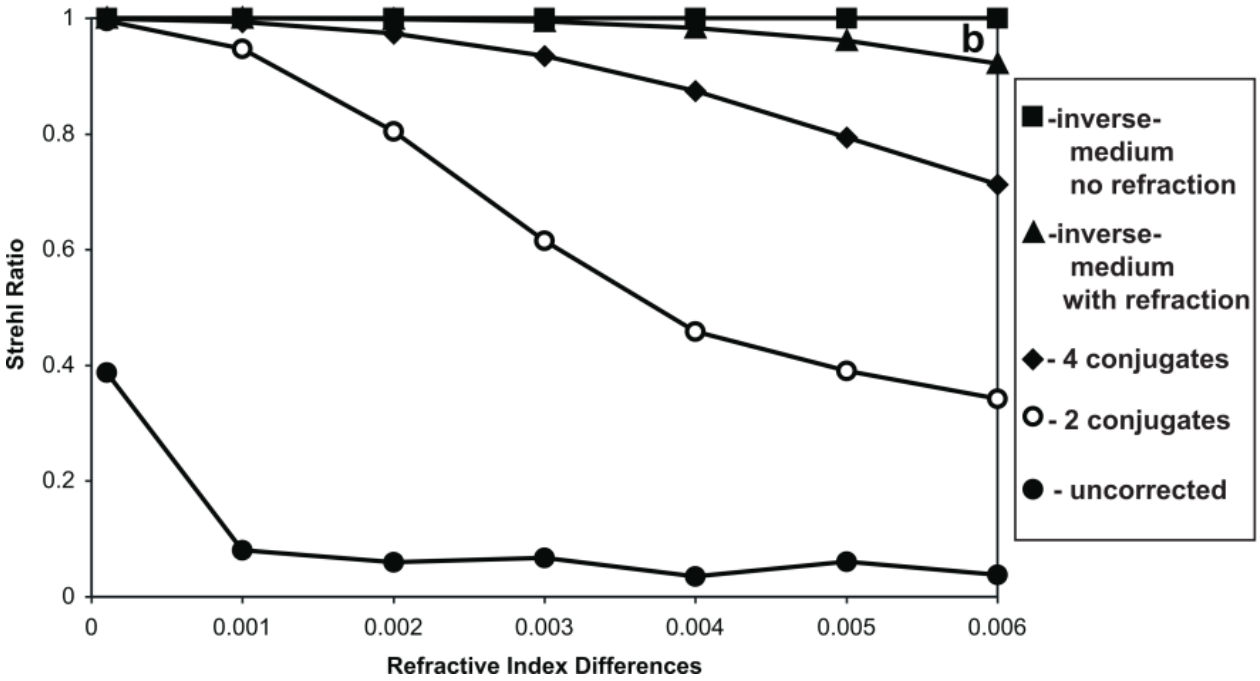

Multiconjugate correction

(a) Correction across the field of view for different multiconjugate adaptive optics schemes. (b) Effect of refractive index differences on different multi-conjugate adaptive optics schemes. The corrections are evaluated by Strehl ratios.

SUMMARY

Good methods to model the microscope PSF
Enable application of these models to correct aberrations
The present limitations to construct the ideal 3D microscope:
    AO technologies